DEVELOPMENT OF A DUOPLASMATRON ION SOURCE AT THE *i*THEMBA LABORATORY FOR ACCELERATOR BASED SCIENCES (*i*Themba LABS)

PETER SETSIPANE MOKODUWE

SUPERVISOR: Dr. J. L. CONRADIE

CO-SUPERVISOR: Mr. J. G. de VILLIERS

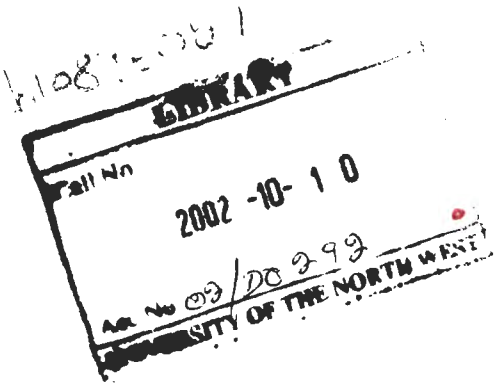

Dissertation submitted in partial fulfillment of the requirements for the degree of Master of Science in Applied Radiation Science and Technology in the Center for Applied Radiation Science and Technology in the Faculty of Agriculture Science and Technology at the University of North-West

February 2002

DEVELOPMENT OF A DUOPLASMATRON ION SOURCE AT THE *i*THEMBA LABORATORY FOR ACCELERATOR BASED SCIENCES (*i*Themba LABS)

PETER SETSIPANE MOKODUWE

***i*Themba LABS, P. O. BOX 722, SOMERSET WEST 7129, SOUTH AFRICA**

FEBRUARY 2002

ABSTRACT

A cold hollow cathode duoplasmatron ion source has been designed, built, optimized and evaluated for use as an external stand-by ion source for the second injector cyclotron (SPC2) during those times that the light-ion injector cyclotron (SPC1) is out of operation and not available for neutron-therapy and the production of radioisotopes, as well as for the Van de Graaff accelerator. In comparison with more elaborate sources a cold cathode source is compact, of small mass, uncomplicated in terms of its construction and easy to operate. It was therefore important to verify whether this type of source can be used for the present application, for which proton beams with intensities of more than 200 μA are required, before the construction of more complex sources should be endeavored.

Since it is difficult to predict the behavior of ion sources by calculation alone, it was considered imperative to build a duoplasmatron source in order to evaluate it experimentally, and at the same time to study the physical processes which occurs in ion sources theoretically, in order to enhance our understanding of the observed source behaviour. The computer program OPERA-3d was used for numerical field calculations and a detailed study of the influence of different operating parameters on the extracted beam current was done to determine the optimum operating conditions of the duoplasmatron ion source. The results lead to a conclusion that more complex and elaborate ion source designs should be considered, because a cold hollow cathode duoplasmatron ion source does not satisfy the beam intensity requirements of neutron-therapy and production of radioisotopes at *i*Themba LABS.

ACKNOWLEDGEMENTS

I want to express my gratitude to Dr. J. L. Conradie for his guidance, advice and excellent supervision in this work, Dr. P. Celliers and Mr. D. Fourie for their assistance with emittance measurements, Mr. G. de Villiers for all the calculations he helped me with and all the effort he put in this work, Mr. H. Delsink for his assistance with drawings, getting parts manufactured and for having his hand ready to help whenever I needed help, and all the members of the group for their valuable contributions towards this project. I also wish to extend my appreciation to Dr. A. H. Botha for his assistance through the writing process.

I also want to thank the *i*Themba LABS for financially supporting the project and the Center of Applied Radiation Science and Technology at the University of North West for exposing me to this exciting field.

Lastly, I want to thank my family, friends and colleagues, without whom none of this would have been possible, for their immeasurable support, love and encouragement. Thank you.

TABLE OF CONTENTS

CHAPTER 1

MOTIVATION AND OUTLINE

1.1 INTRODUCTION

*i*Themba Laboratory for Accelerator Based Sciences (*i*Themba LABS), formerly known as the National Accelerator Centre (NAC) **[RAU75, REP75],** is a multidisciplinary research centre, which provides beams of accelerated charged particles and facilities for particle radiotherapy, basic and applied nuclear physics research and the production of radioisotopes for nuclear medicine and industry.

The laboratory, which became operational during 1986, operates a 200 MeV separated-sector cyclotron (SSC) and two solid-pole injector cyclotrons, SPC1 and SPC2, for pre-acceleration of light ions and heavy ions, respectively, before final acceleration in the SSC. These machines and their associated beamlines were custom designed at *i*Themba LABS.

The SPC1 has an internal ion source, capable of delivering intense beams of light ions and is mainly used for acceleration of proton beams for proton and neutron-therapy as well as for the production of radioisotopes. Light and heavy beams produced in an external electron cyclotron resonance (ECR) ion source and polarized protons from a second external ion source are accelerated in SPC2 before injection into the SSC. SPC1 and SPC2 are solid-pole cyclotrons with maximum proton energies of 8 MeV. The beam energies of all three machines can be varied over a wide range: a factor 10 for protons in the case of the SSC.

In addition to the three cyclotrons a commercially acquired 6 MV CN Van de Graaff accelerator, capable of delivering beams of light and heavy ion with a low energy spread, is also in operation at *i*Themba LABS. The Southern Universities Nuclear Institute

(SUNI), which has been incorporated into *i*Themba LABS, commissioned this machine in 1963.

The energy, quality and intensity of beams delivered by accelerators depend to a large extent on the charge state and intensity that can be obtained from the ion source. In the case of cyclotrons the maximum attainable beam energy is proportional to the square of the charge state. Ion source development, which is the main theme of this study, therefore forms an important part of the activities of an accelerator laboratory.

1.2 MOTIVATION

From time to time, when SPC1 is out of operation, SPC2 is used for pre-acceleration of proton beams for neutrontherapy and the production of radioisotopes. These applications require relatively high-intensity proton beams of between 30μA and 150μA. With the ECR source the maximum beam intensity obtainable from SPC2 is 60μA. With the polarized ion source it is even less. The need for an external ion source, capable of delivering high-intensity proton beams of good quality, for injection into SPC2 therefore exists at *i*Themba LABS. Various types of ion sources, i.e. duoplasmatron, Penning Ionization Gauge (PIG) and multi-cusp have been considered for this purpose. Since a duoplasmatron ion source is by far the most simple and compact in terms of construction, and also the cheapest, it has to be considered for the present application.

Since the description of a duoplasmatron ion source by von Ardenne [**ARD56**] in 1956, this type of source have been widely used in different fields [**ADB90, KOL98, SCH97, QAY94 ZHO81**] as sources of intense ion beams. Although duoplasmatron sources can be build with either hot or cold cathodes, hot filament sources are predominantly in use because of the good quality beams resulting from the high ionization efficiency obtained from excitation with electrons of high temperature and density. Hot cathode sources have, however, short lifetimes due to sputtering of the filament as a result of the inevitable bombardment with positive ions. Hollow cathode duoplasmatron ion sources [**BAT74, KER92**] operate without a filament and therefore have long lifetimes. These types of duoplasmatron source have the following characteristics:

- High ionization efficiency
- High current density
- It can yield a good quality beam
- Increased lifetime
- Compactness and simple geometry
- Inexpensive

Since it is difficult, if not impossible, to calculate the complex behavior of a plasma in an ion source, due to amongst others the complexity of the boundary conditions of the magnetic field, it was decided to design, construct and build a hollow, cold cathode, duoplasmatron ion source at *i*Themba LABS in order to evaluate it experimentally in terms of purity of beam, intensity, energy spread and horizontal and vertical emittance.

The main objective of this study is therefore to develop a duoplasmatron ion source that can deliver proton beams of at least 200μA but preferably 500μA to be used as a stand-by ion source for the SPC2. The transmission from the ion source through SPC2 is 30%. A source with small dimensions, lightweight and simple geometry will not only be suitable for use with SPC2 but also for the Van de Graaff accelerator at *i*Themba LABS. In the Van de Graaff accelerator the ion source is situated in the high-voltage terminal, which makes water-cooling extremely difficult. Because of this it was decided to cool the source only by conduction through its supporting structure to the ambient atmosphere and not to use any form of forced cooling.

Should the evaluation show that the duoplasmatron ion source does not meet the requirements, more elaborate and expensive ion source such as a multi-cusp ion source will have to be considered, with the certainty that the simpler and cheaper option of a duoplasmatron sources have been eliminated on solid grounds after proper investigation. Valuable experience will be gained by developing the duoplasmatron source, which will be of great value for future development work at *i*Themba LABS.

1.3 OUTLINE OF DISSERTATION

The basic structure of the dissertation is as follows:

- The facilities at *i*Themba LABS are described briefly in chapter 2.
- A general discussion on plasma sources, in widespread use at present, as well their discharge mechanisms and beam extraction processes, is given in chapter 3.
- In chapter 4, a description of the processes taking place in a plasma, including a more detailed analysis of the influence of different parameters, as for example the magnetic field distribution, on the plasma behaviour, is given.
- The design considerations, construction and development of the duoplasmatron ion source at *i*Themba LABS are discussed in chapter 5.
- Optimization of the source performance and the results obtained are presented in chapter 6. The influences of the different operating parameters like arc current, extraction voltage, gas pressure, etc. are discussed.
- The emittance and the measurement techniques thereof are discussed in detail in chapter 7.
- Finally, the conclusions drawn from this study and recommendations for further work on ion sources at *i*Themba LABS are given in chapter 8

CHAPTER 2

THE ACCELERATOR FACILITIES AT *i*Themba LABS

2.1 INTRODUCTION

During the late nineteen sixties and early nineteen seventies it became clear that the then existing accelerator facilities in the country did not meet the requirements for nuclear physics research, particle radiotherapy and the productions of radioisotopes. The main accelerators in operation at that stage were the variable-energy cyclotron at the Council for Scientific and Industrial Research (CSIR) and the 6MV Van de Graaff accelerator of the Southern Universities (SUNI) near Faure. The locally built CSIR cyclotron could accelerate light ions to the following maximum energies: 15.3 MeV for protons, 17 MeV for deuterons, 34 MeV for alpha particles and 39 MeV for Helium-3 ions. Deuteron and Helium-3 beams, which at that time were available at a only few cyclotron laboratories in the world, were, apart from nuclear physics research, also used for the production of radioisotopes for South African hospitals and industries. Some of these isotopes were also exported and were, amongst others, used as a power source in the Mariner spacecraft.

Experience gained with the construction and use of the CSIR cyclotron gave physicists the confidence to start with the design of a new separated-sector cyclotron. Due to a lack of funds, South African nuclear physicists and radiotherapists decided to investigate whether a single multi-disciplinary facility, capable of meeting the requirements of nuclear physics, particle radiotherapy and production of radioisotopes, could be designed and built. As a result of the feasibility study, the facilities described below, have been established by the CSIR. The project was approved in 1977 and the first proton beam was accelerated to an energy of 66 MeV, at the extraction radius of the SSC, in October 1985. The maximum design energy of 200 MeV was achieved in March 1986.

2.2 THE *i*Themba LABS CYCLOTRON FACILITIES

Figure 2.1 shows the layout of the three cyclotron vaults and the user areas at *i*Themba LABS. Beams of charged particles are transported from the external ion sources to SPC2 and after pre-acceleration from SPC1 and SPC2 to the SCC for final acceleration. From the SSC the beams are directed to the areas and vaults for nuclear physics research, proton- and neutrontherapy and production of radioisotopes. In the regions between accelerators, as well as from the accelerators to the users, the beam moves through evacuated stainless-steel beam pipes. Beam focusing with the large number quadrupole magnets, which will be seen in **figure 2.1**, prevents lateral spread-out of the beam, whereas dipole magnets are used to change the beam direction. Concrete walls with a wall thickness of 4.5m provide protection to human beings and sensitive equipment against the radiation generated at points where the beam strikes accelerator components and beam targets.

2.3 THE VAN DE GRAAFF FACILITIES

The layout of the Van de Graaff facilities is shown in **figure 2.2**. Beams with variable energy, and a maximum value of 6 MeV for protons, are delivered to several target stations, amongst others, for solid-state physics research, the micro-probe facility and for Particle Induced X-ray Emission (PIXE). With a Van de Graaff accelerator the beam energy can be varied quickly and the energy spread in the beam is small in comparison with unanalyzed cyclotron beams. As in the case of the cyclotron facilities, the main beamline elements consist of quadrupole and dipole magnets.

2.4 THE SEPARATED-SECTOR CYCLOTRON (SSC)

The layout of the SSC is shown in **figure 2.3**. The beam energy is variable and although the maximum design energy for protons is 200 MeV, protons have occasionally been accelerated to 227 MeV for special purposes. Four separate magnet sectors, each with a mass of 350 tons, a sector angle of 34 degrees and a maximum field strength of 1.256T, ensure that the beam passes repeatedly, up to 350 times, through the two $\lambda/2$-resonators with a frequency range of 6 to 26 MHz and a maximum dee voltage of 220 kV. The two resonators are capacitively coupled to two 150 kW power amplifiers. The dee voltage and

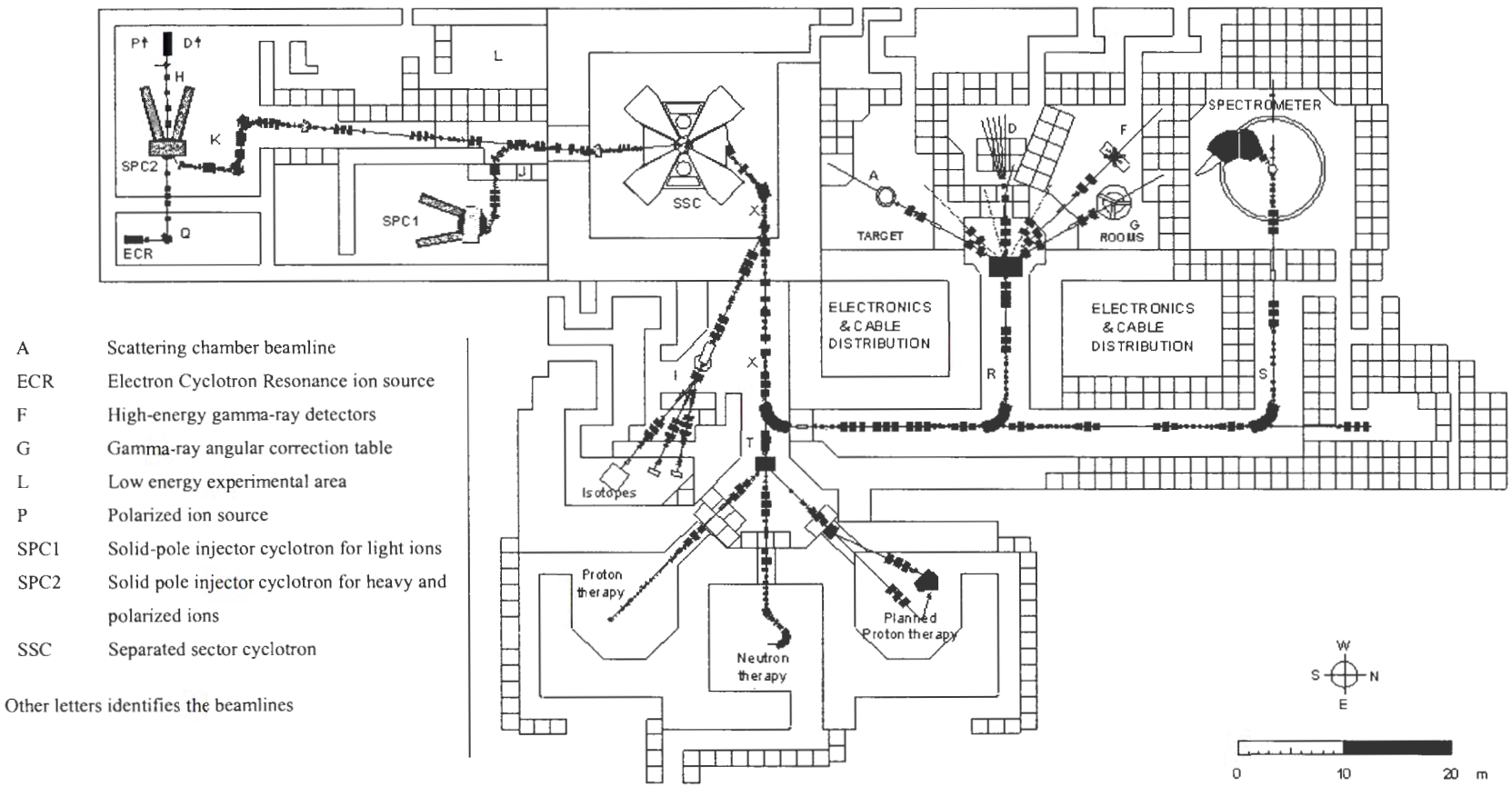

A	Scattering chamber beamline
ECR	Electron Cyclotron Resonance ion source
F	High-energy gamma-ray detectors
G	Gamma-ray angular correction table
L	Low energy experimental area
P	Polarized ion source
SPC1	Solid-pole injector cyclotron for light ions
SPC2	Solid pole injector cyclotron for heavy and polarized ions
SSC	Separated sector cyclotron

Other letters identifies the beamlines

Figure 2.1: Layout of the *i*Themba LABS facilities

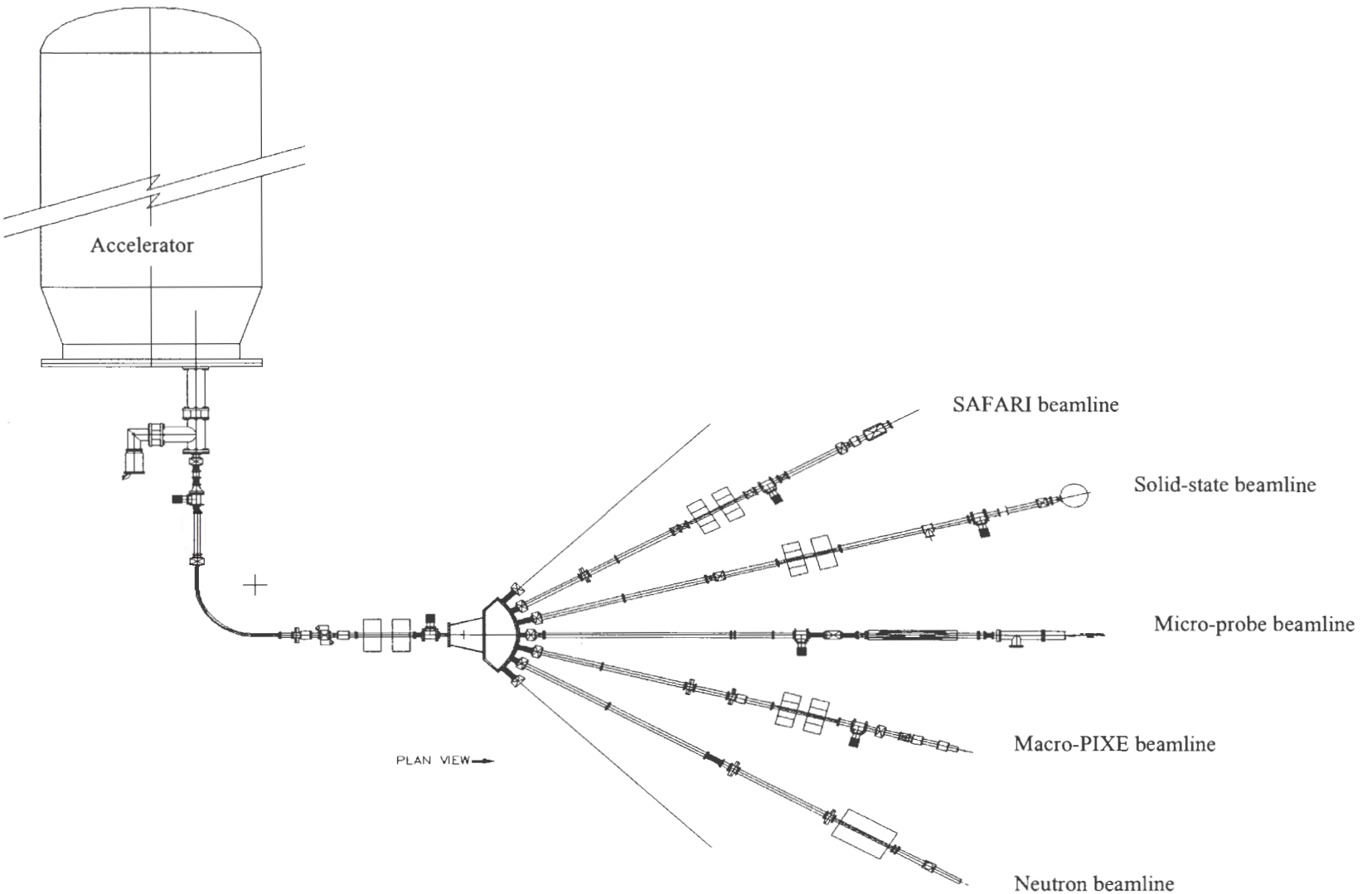

Figure 2.2: Layout of the Van de Graaf facilities at *i*Themba LABS

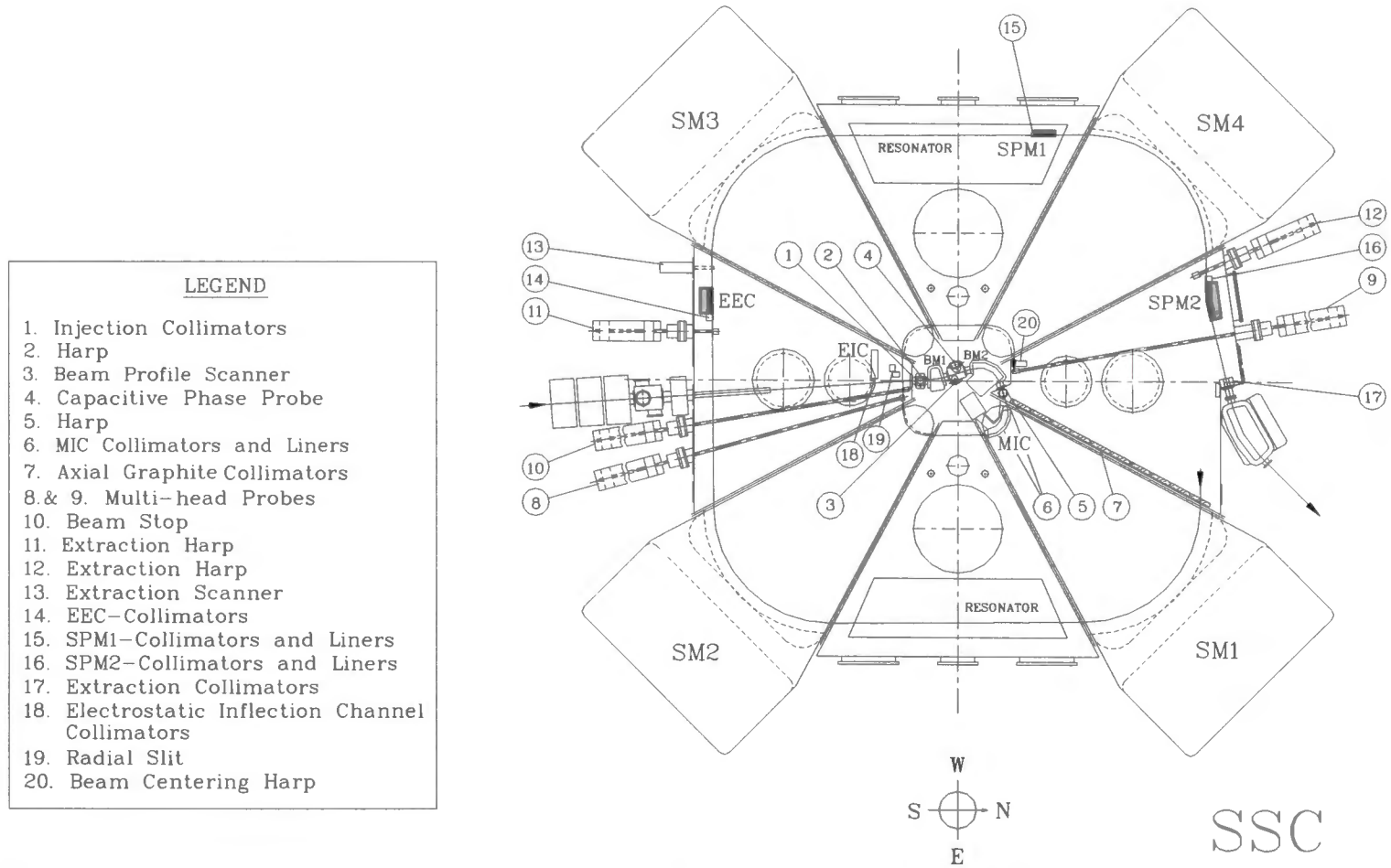

Figure 2.3: Layout of the separated-sector cyclotron (SSC) at the *i*Themba LABS

phase is stabilized with feedback systems. Another feedback system also compensates for beam loading and temperature changes in order to keep the high Q-value resonators tuned. Similar feedback systems are used for the injector cyclotrons.

The injection system consists of two bending magnets and a magnetic inflection channel. The beam is extracted with two septum magnets. An electrostatic extraction channel is also available but has seldom been used. The large spaces between magnet sectors allow resonators with high dee voltages to obtain good orbit separation at extraction. Since the dees are outside the magnet pole gaps it is possible to use small pole gaps in order to obtain strong vertical beam focusing. The small pole gap of 66 mm ensures that the magnetic field strength drops off sharply at the extraction radius. Beam extraction is much easier than in the case of solid-pole cyclotrons, because of the sharp drop in the field strength and the relatively large spaces between the magnet sectors available for extraction components.

The SSC accelerates beams of light and heavy, up to Xenon, ions as well as beams of polarized protons. Proton beam intensities of more than 100 μA, at 66 MeV, are extracted from the SSC for the production of radioisotopes. Activation of the components of the SSC, and the consequent risk for staff during maintenance, are limited, as a result of the high extraction and transmission efficiency of the SSC, which is more than 99.7%.

2.5 THE LIGHT-ION INJECTOR CYCLOTRON (SPC 1)

Figure 2.4 shows the layout of the light-ion injector cyclotron, SPC1. The H-type solid-pole magnet has four 45^0 radial sectors, for vertical focusing, attached to each of the poles. The internal Penning Ionization Gauge (PIG), source is situated in the center of the pole gap. The acceleration system consists of two $\lambda/4$ resonators, with two 90^0 dees, coupled to two 20 kW power amplifiers. The beam is extracted, at a radius of 0.476 m, with an electrostatic channel and two magnetic channels.

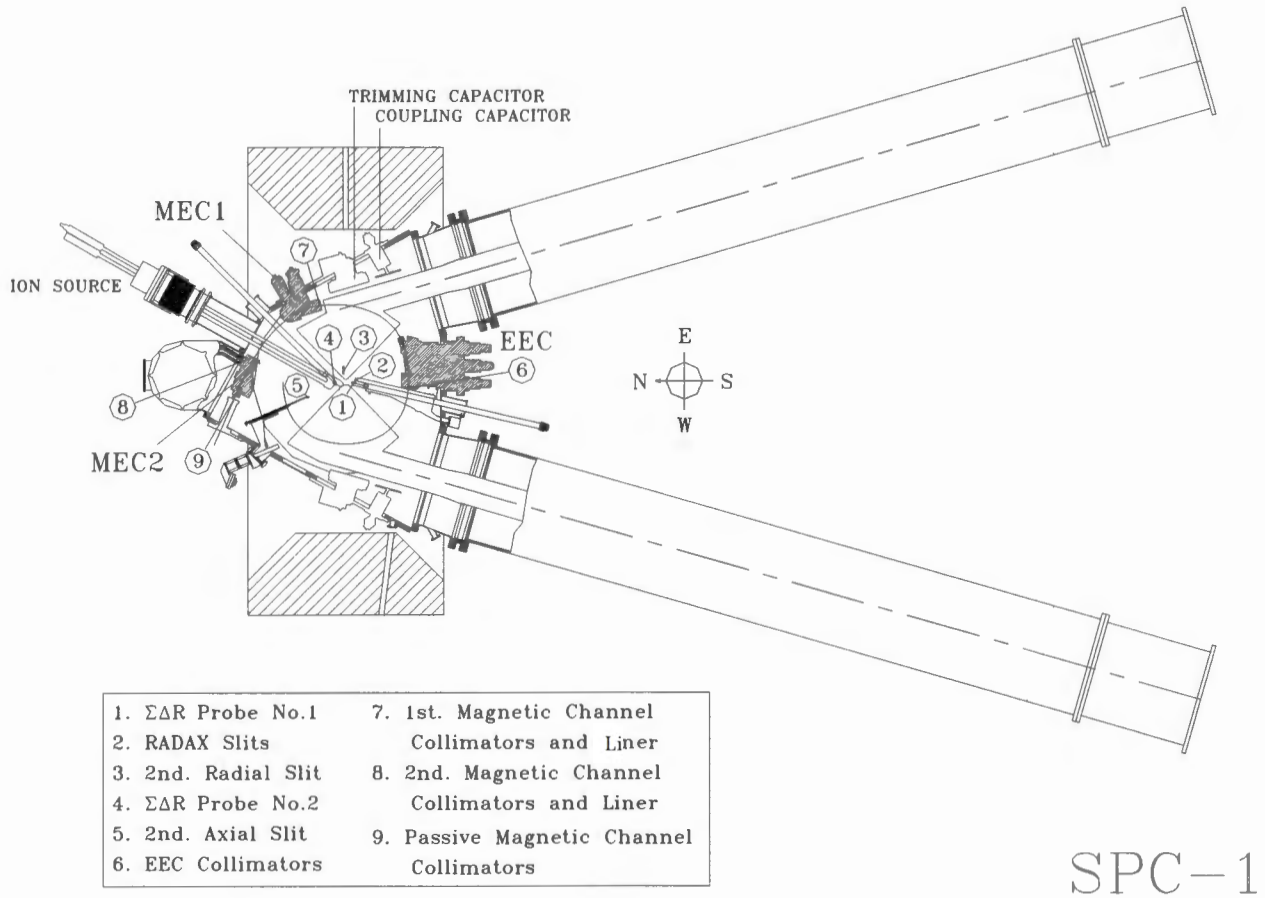

Figure 2.4: Layout of the light ion injector cyclotron (SPC1)

2.6 THE INJECTOR CYCLOTRON FOR HEAVY AND POLARISED HYDROGEN IONS (SPC2)

Figure 2.5 shows the layout of the injector cyclotron for polarized and heavy ions, SPC2. Apart from the axial injection system, SPC2 is very similar to SPC1. Again, the H-type solid-pole magnet has four 45^0 radial sectors and the acceleration system consists of two $\lambda/4$ resonators, with two 90^0 dees, coupled to two 20 kW power amplifiers. The beam is also extracted, at a radius of 0.476 m, with an electrostatic channel and two magnetic channels. The layout of the two external ion sources, the Electron Cyclotron Resonance source and the polarized hydrogen ion source, and their beamlines are shown in **Figure 2.6**. The beam is inflected into SPC2 with an electrostatic spiral inflector. Both quadrupole and solenoid magnets are employed for focusing in the beamlines. The proposed position for the duoplasmatron is shown in **figure 2.6**.

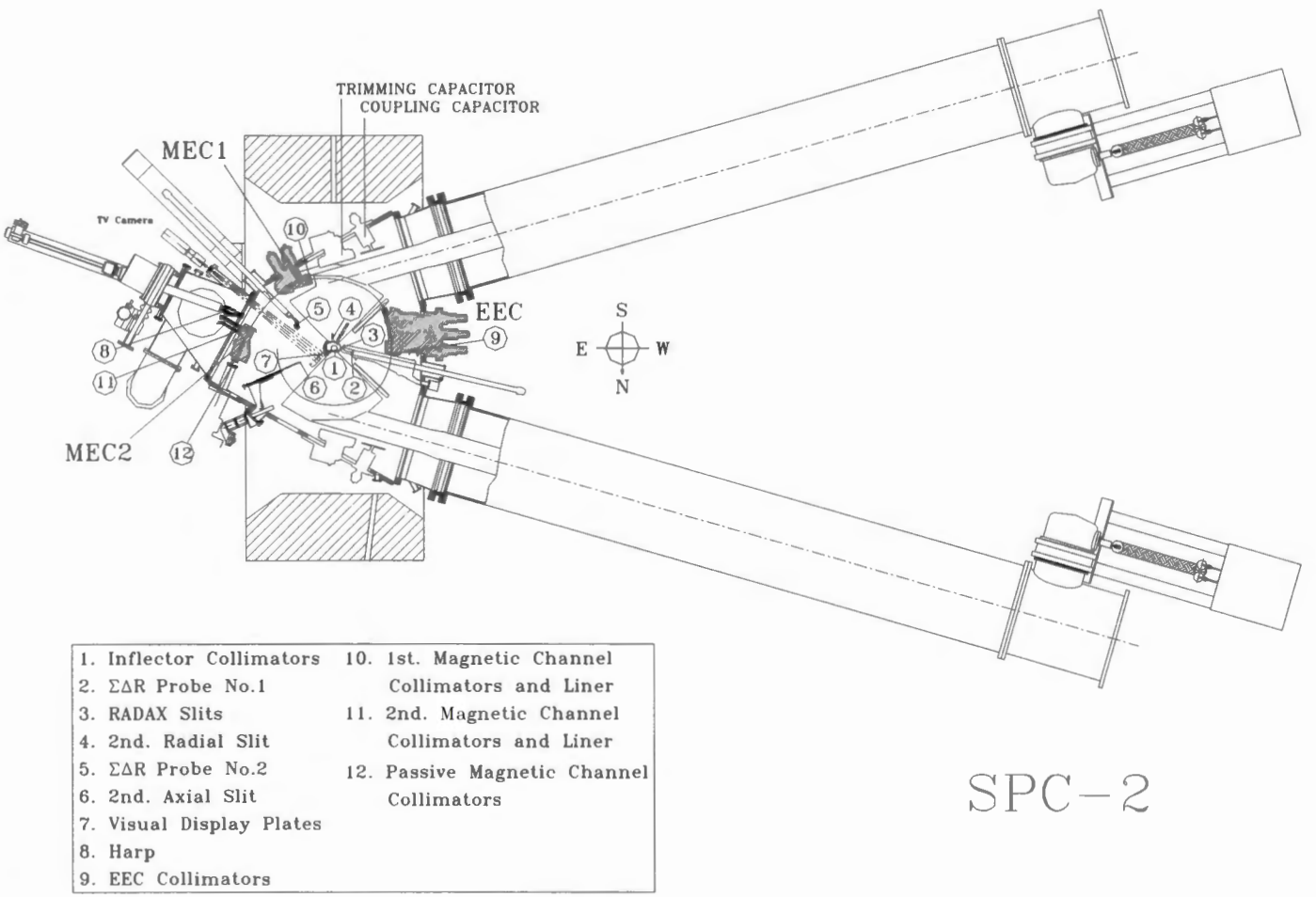

Figure 2.5: Layout of the polarized and heavy ion injector cyclotron (SPC2)

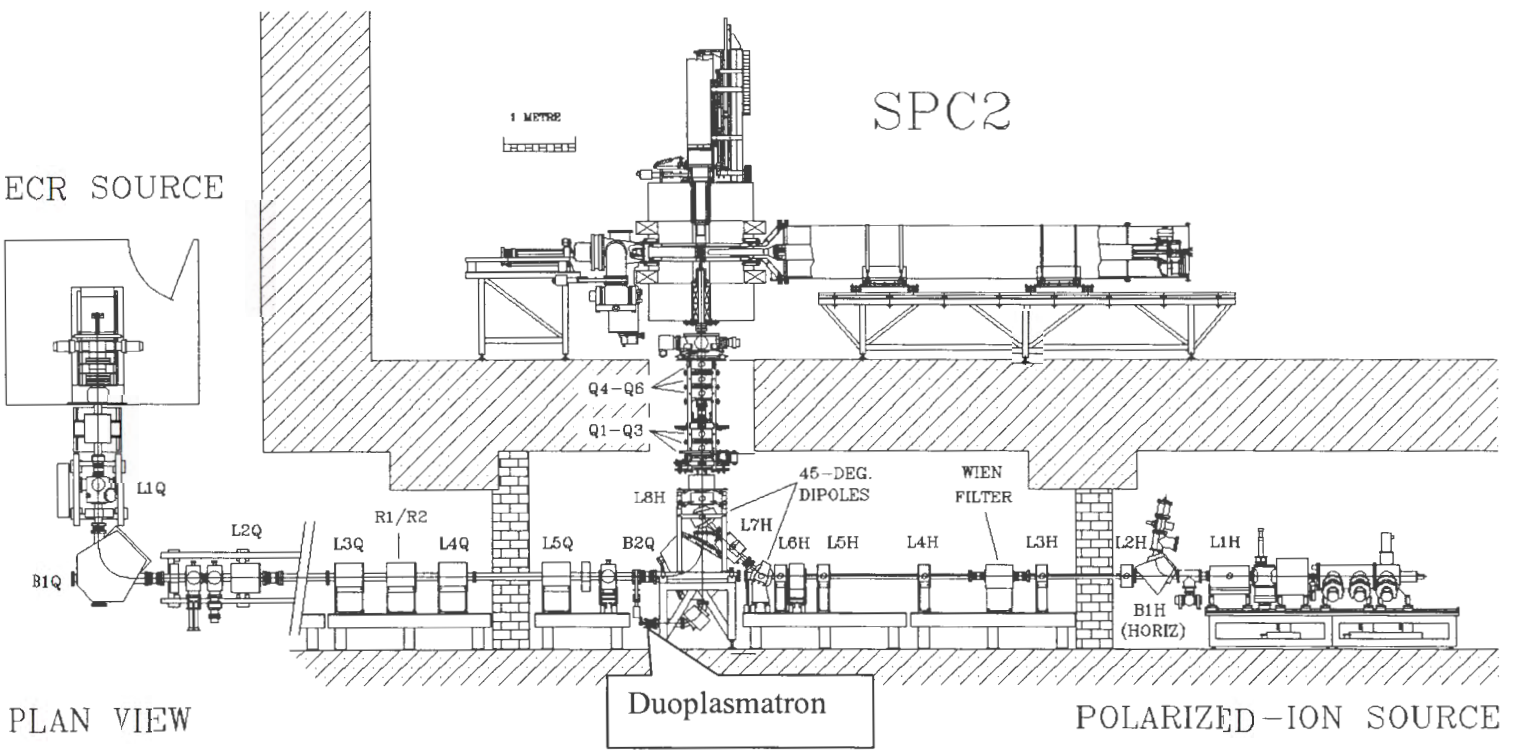

Figure 2.6: Diagram showing the two ion sources presently used at the SPC2 and the planned position for the duoplasmatron

CHAPTER 3

GENERAL OVERVIEW OF PLASMA ION SOURCES

3.1 INTRODUCTION

Plasma ion sources can be classified in two main families: arc plasma [**BEN76**] and plasma confinement sources [**GEL76**]. Many different types of plasma sources are available and the choice of a suitable source depends on the beam requirements of the application, such as intensity, duty cycle and beam emittance, as well as on more practical considerations such as size, cost, complexity of construction and ease of operation. A brief description of the major ion sources, currently in use at accelerator laboratories, their operating principles and characteristics are given in this chapter.

3.2 ARC SOURCES

3.2.1 PENNING IONIZATION GAUGE (PIG) SOURCE

Both hot and cold cathode PIG ion sources are in use in cyclotrons. Because of the severe sputtering of the hot and fragile filament by heavy ions, and the consequent short filament lifetimes, hot cathode sources are mainly used for the formation of light ions, such as in the case of SPC1. Cold cathode sources are more difficult to start and require higher voltages, but the cold cathodes are more resistant than a filament against sputtering and are therefore more suitable for heavy ion acceleration. In cold cathode sources sputtering is often used to vaporize non-volatile elements to be ionized in the discharge.

A later development of hot cathode sources was to use an indirectly heated cathode, instead of a filament as cathode, in order to protect the filament against sputtering. A schematic drawing of an indirectly heated hot cathode PIG source, such as the one in SPC1, is shown in **figure 3.1**. The source consists of a hollow anode, into which the gas

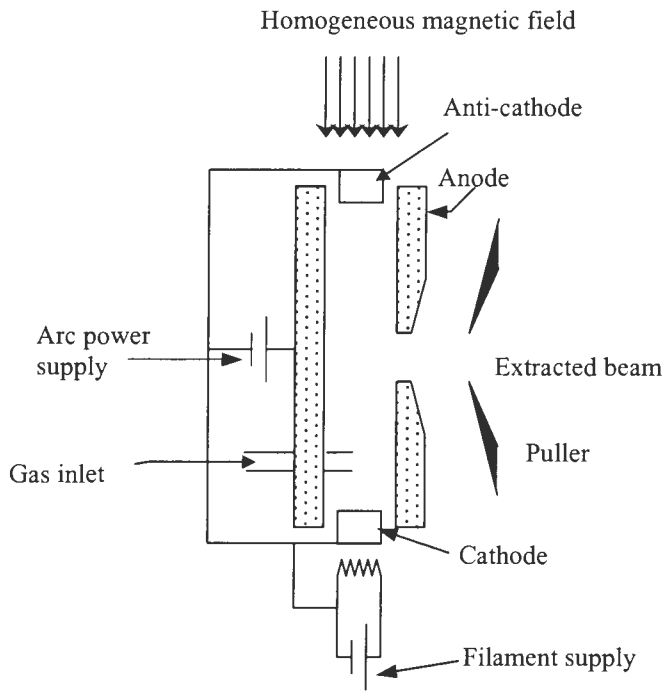

Figure 3.1: A schematic diagram of a PIG ion source and its power supplies

to be ionized flows at a regulated low pressure, an indirectly heated cathode and an anticathode, all positioned in the almost homogeneous magnetic field of the cyclotron.

Electrons, generated by thermionic emission at the cathode, are accelerated into the hollow anode where they collide with gas molecules, thereby causing dissociation of the gas molecules and ionization of the atoms. Entering the space between the anode and anticathode electrons are retarded and then accelerated back into the anode. However, positive ions entering these spaces are accelerated towards the cathode and anticathode and cause sputtering.

Electrons, emitted with a velocity component perpendicular to the magnetic field, follow spiral orbits through the aperture of the anode and are prevented from colliding with the

anode. A large fraction of the electrons is therefore trapped axially by the electrostatic well and radially by the magnetic field. Continued reflection of electrons into the anode plasma by the electrodes at each end of the anode and the increased length of the electron paths through the anode due to their spiral shape result in an increased interaction probability and a very dense plasma [**TON87, CON92**].

Typically the anode power supplies operates at about 100 V and a current of 2 A, for a gas flow of 10 cc at N.T.P. (normal temperature and pressure) but higher voltages, up to 600 V are required for ignition of the arc. The filament power supply typically operates with a current of 180 A and about 5 V across the filament. Higher currents, about 200 A, are required to ignite the discharge. Under these conditions proton beams of several mA can be extracted from the source, either through a slit in the anode or axially through a small hole in the center of one of the cathodes.

The cathodes of PIG sources have relative short lifetimes due to their exposure to sputtering. Maintenance has therefore to be done every three to four days. Since ion source materials such as Tungsten, Tantalum, Molybdenum and Lanthanum-Hexaboride are expensive, operational cost is not negligible. PIG sources are generally large and are suitable for high duty factor operation [**BRO89**] especially when used as an external source for a cyclotron in which case an additional magnet has to be provided.

3.2.2 DUOPLASMATRON ION SOURCE

The duoplasmatron ion source was first designed and built by Von Ardenne [**ARD56**] and is utilized for scientific research and a variety of industrial applications [**ADB90, KOL98, SCH97, QAY94 ZHO81,**]. The source can be adapted to suit the requirements of a wide variety of users in different fields. Both cold and hot cathode sources are in use. **Figure 3.2** shows a schematic diagram of a hot cathode duoplasmatron source and its power supply connections for the case where it would be used as an external ion source for an accelerator.

As the name indicates the discharge is formed in two-stages: the first between the filament, which acts as cathode, and the intermediate electrode at a relatively high pressure and low voltage [**BRO89**], and the second between the intermediate electrode and the anode. Electrons, generated by thermionic emission at the cathode, are accelerated towards the anode and along the way collide with gas molecules, thereby causing dissociation of the gas molecules, ionization of the atoms and formation of a plasma in the region between these electrodes.

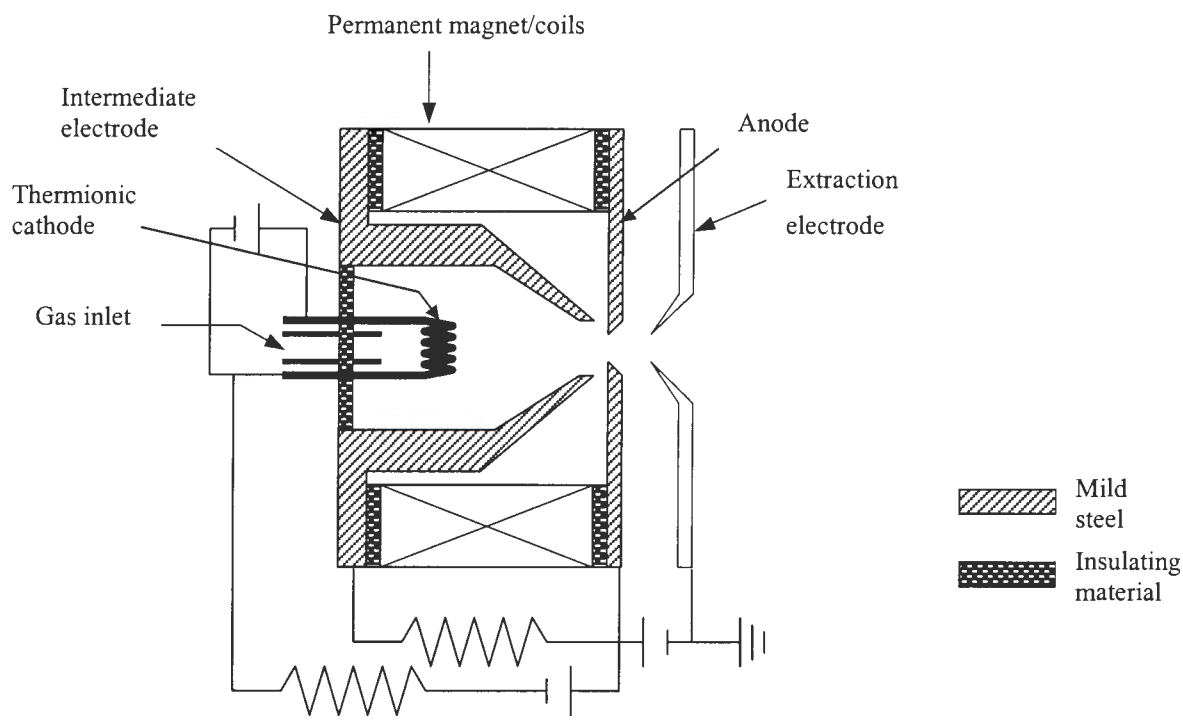

Figure 3.2: A schematic diagram of a hot cathode duoplasmatron ion source

The electrical field, due to the voltage difference between the cathode and the intermediate electrode, shifts the plasma towards the anode. The strong magnetic field guides the plasma to flow through the orifice in the intermediate electrode into the second stage where another plasma is formed between the intermediate electrode and the anode. A combination of the magnetic and the electric fields are employed to constrict the motion of electrons and ions [**HIL**] through the anode aperture and thus increasing the interaction cross-section resulting in increased ionization.

In the second stage the discharge pressure is much lower and the voltage much higher than in the first stage. The anode has a small aperture through which the plasma flows into the extraction region. The geometry of these electrodes can be varied to optimize the output of the ion source. Expansion cups can also be fixed to the anode to allow the plasma to expand before extraction [**KOV71**] and this can improve the extracted beam current. Typical discharge voltages and currents are up to few hundred volts and a few ampere.

3.3 PLASMA CONFINEMENT SOURCES

3.3.1 ELECTRON CYCLOTRON RESONANC (ECR) ION SOURCE

ECR sources, invented by Geller [**GEL96, BRO89**], are widely used for the production of high-quality heavy ion beams, due to their reliability and the high charge states that can be obtained from them. For a cyclotron of a given size and magnetic field strength the maximum beam energy is proportional to the square of the charge state of the ion. It is therefore worthwhile to invest in an ion source capable of delivering beams of ions with high charge states at sufficient intensities. For the acceleration of heavy ions PIG sources have consequently almost completely been replaced with ECR sources.

An ECR source can be operated over periods of weeks without requiring maintenance because no filaments and cathodes, which can be damaged by sputtering, are used in the source. Only the gas fed into the source for ionization is consumed. For the ionization of non-volatile elements, however, either a volatile chemical compound of element has to be prepared or a rod of the material has to be inserted in the source for vaporization by sputtering.

Figure 3.3 shows the layout of an ECR source and the distribution of the axial magnetic field strength along horizontal centerline of the source. This field distribution, also known as a minimum-B configuration, is obtained by combining the axial magnetic field of suitably arranged Helmholtz coils, for horizontal confinement of the plasma, with the field of radial multipole magnets, usually hexapoles, for radial confinement of the

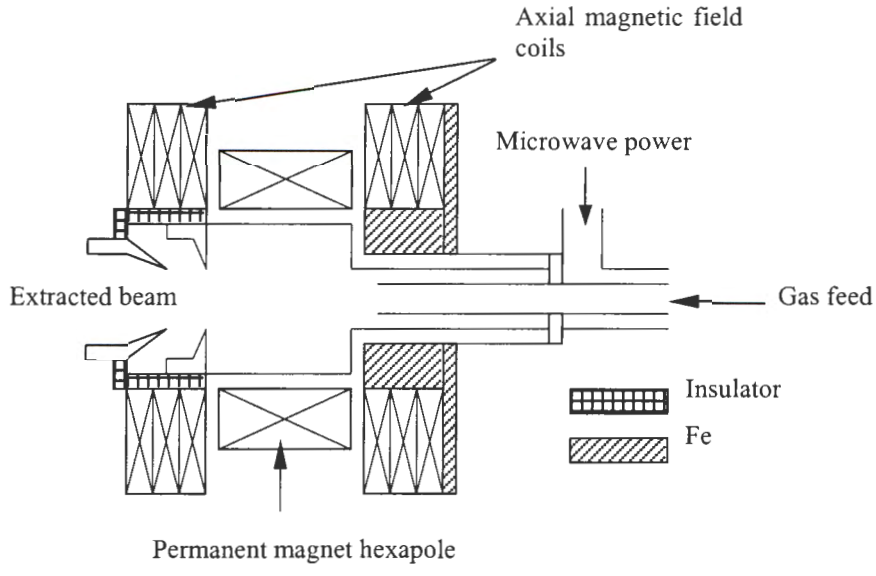

Figure 3.3a: A schematic diagram of a typical ECR ion source.

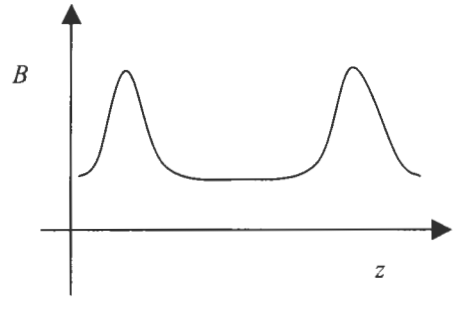

Figure 3.3b: The typical magnetic field profile in the ECR ion source

plasma. This field distribution keeps particles in the plasma for long confinement times. Particles which approach the axial extremities of the plasma, where the magnetic field has a maximum value, are reflected back into the plasma by the magnetic mirrors, which are formed by the minimum-B field distribution. They can escape from their magnetic confinement only when their angle of approach with respect to the axis is small enough.

In an ECR source electrons do not gain energy by electrostatic acceleration, as is the case in the previously discussed sources, but from a microwave electromagnetic field, fed into the vacuum chamber inside the magnet, through a window, which is transparent at the microwave frequencies. The microwave frequency, f, is chosen to satisfy the cyclotron resonance condition:

$$f = \frac{eB}{2\pi m} \tag{1}$$

where

e: is the electron charge

B: is the magnetic field strength and

m: is the electron mass.

Since the magnetic field in the plasma region of the source is not constant, this resonance condition is satisfied on a surface only. Electrons passing through this surface are accelerated by the microwave field and thereby gain energy required to ionize the gas. An electron with velocity, v, will move in an orbit with radius r, given by:

$$r = \frac{mv}{eB} \tag{2}$$

and passes many times through the surface at which the resonance condition is satisfied and thus accelerated sufficiently to ionize gas atoms to high charge states. The ECR and their peripheral equipment such as power supplies, microwave generators and vacuum systems are expensive and complex and are therefore mainly utilized for acceleration of heavy ions and as ionizers for polarized ion sources.

3.3.2 MULTI-CUSP ION SOURCE

Figure 3.4 shows the layout of a multi-cusp source and its power supply connections for use as an external ion source for a cyclotron. It is a single-stage discharge source. The discharge chamber, which is also the anode of the source, is practically surrounded by arrays of permanent magnets to produce a multi-cusp magnetic field for containment of the plasma [**BRO89**]. Primary electrons are generated by thermionic emission at the

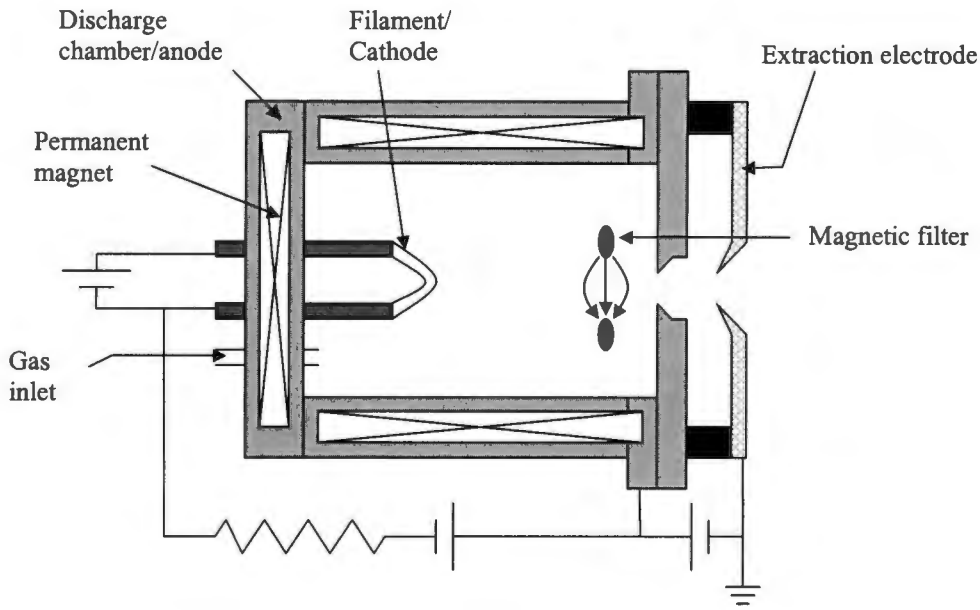

Figure 3.4 A schematic diagram of a multi-cusp ion source.

filament, which is also the cathode of the source, and are accelerated by the electrostatic field in the region between the cathode and anode, created by the voltage applied between these electrodes.

The magnetic field not only confines the plasma, but also increases the path lengths of the ionizing electrons and reduces their drift to the anode walls. Increasing the field strength at the ends of the confinement region can reduce plasma losses. Positive ions are extracted from the discharge by a negatively biased extraction electrode. The magnetic filter in the source is used to reduce recombination in the extraction region. Positive ions are also accelerated towards the filament, which is in general a fragile element component, and causes sputtering. The source therefore requires regular maintenance.

Multi-cusp sources have sufficient space to allow installation of more than one filament, of which only one is connected to the power supplies, at a time. When one filament is

damaged the power supplies can be quickly switched over to another one, in order to limit down time of the accelerator. In some multi-cusp sources an RF antenna is used as a cathode, instead of a filament. In such sources it is more difficult to ignite the discharge and the gas in the discharge chamber is often irradiated with ultra-violet light to start the discharge. The RF antenna has also to be carefully matched to the plasma and variations in the discharge conditions require re-adjustment of the matching network. The main advantage of multi-cusp sources is that they are capable of delivering very high intensity beams of good quality. In general they are, however, considerably more expensive and of a more complex construction than a cold cathode duoplasmatron source.

3.4 SUMMARY

From the description of the various sources above and discussion of their characteristics it follows that the duoplasmatron is the simplest in terms of construction and also the cheapest and has consequently to be considered as a first option for the present application.

CHAPTER 4

THE THEORY OF THE PHYSICAL MECHANISMS IN A DUOPLASMATRON ION SOURCE

4.1 INTRODUCTION

The physics of ion sources is complex and the behaviour of ion sources can seldom be predicted exactly by theory. This may be attributed to the unique behaviour of a plasma. In this chapter, the attention will be primarily on the behaviour of the plasma in the source. A theoretical description of the mechanisms involved in the formation of the plasma, the extraction and the axial transport of charged particles through the dual confinement will be given. These processes collectively determine the ion beam quality at extraction.

4.2 GENERAL CHARACTERISTICS OF THE DUOPLASMATRON DISCHARGE

The discharge is maintained at relatively high pressure and low voltage between the cathode and an intermediate electrode [**BRO89**]. The discharge plasma is sustained by both the axial magnetic field and the electrons that are emitted by the cathode and radially constricted by the intermediate electrode (IE), which is located between the cathode and anode. The axial magnetic field acts to align the electrons. The potential distribution in the plasma is shown in **Figure 4.1**. Electrons are accelerated in the region of the cathode voltage drop, V_k in the direction of the IE. The constriction by the IE generates a potential discontinuity in the discharge. Ionization is mainly due to inelastic collisions between electrons with a Maxwellian velocity and the gas atoms. Maxwellian velocity distribution will be discussed in the next section.

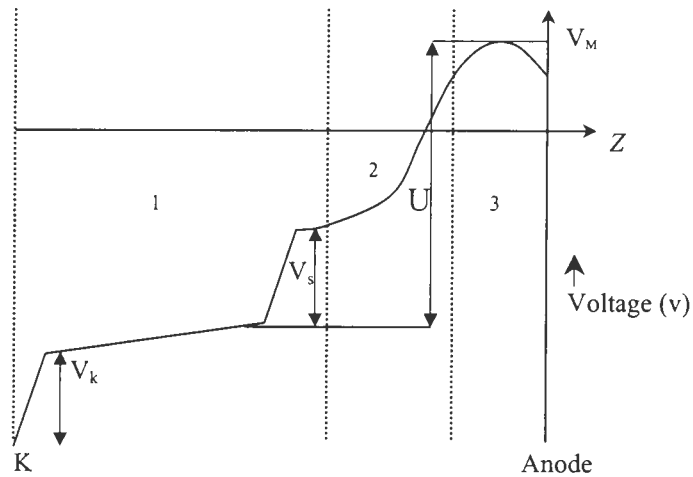

Figure 4.1: Idealized potential distribution along the discharge axis in the normal arc mode. (1)-Cathode plasma. (2)-Intermediate plasma. (3)-Anode column. V_k-cathode fall. V_s-potential jump in the constriction sheath. V_M-anode fall. U-energy of primary electrons.

An equipotential cathode plasma, required for arc conduction in the cathode discharge, is insured by the formation of a sheath on the cathode and another constriction sheath on the IE. The potential jump, V_S, is as a result of the formation of a space-charge double layer at the IE entrance. The anode fall, V_M, corresponds to the refection of secondary electrons and the acceleration of the positive ions towards the anode **[LEJ71]**.

4.3 DISTRIBUTIONS IN THE PLASMA

The temperature, velocity and energy distribution of particles in the plasma are also important parameters. In the absence of external influences or forces plasma will tend to be in thermal equilibrium and thus have particles of different velocities. The distribution of these velocities is Maxwellian and is given by,

$$f(u) = n\left(\frac{m}{2\pi KT}\right)^{3/2} \exp\left[-\frac{1}{2}mu^2 / KT\right] \quad (3)$$

where

$f(u)$	=	distribution function
n	=	density, in particles per cm^3 and is given by
		$n = \int_{-\infty}^{\infty} f(u)du$ (4)
T	=	plasma temperature in K
$f(u)du$	=	number of particles per cm^3 with velocity u and $u + du$
K	=	Boltzmann's constant
	=	$1.38 \times 10^{-23}\ J/K$
$\frac{1}{2}mu^2$	=	Kinetic energy of the particles
m	=	mass of the atomic species involved

In one dimension

$$f(u) = n\left(\frac{m}{2\pi KT}\right)^{1/2} \exp\left[-\frac{1}{2}mu^2 / KT\right] \quad (5)$$

The function $f(u)$ gives a description of the distribution of particle velocities.

The plasma temperature, T, determines the width of the distribution. It is possible to have ions and electrons with different Maxwellian distributions and with different temperatures T_i and T_e. This is as a result of the different collision rates amongst particles.

Plasmas are known for not conforming to applied electric potentials, because of its shielding effect to external electrostatic field is applied to a plasma, particles are redistributed so as to cancel the effect of the applied field. The distance in the plasma over which the effect of external influences is totally screened out is called the Debye length, denoted by λ_D and is given by

$$\lambda_D = \left(\frac{KT_e}{4\pi ne^2} \right)^{1/2} \tag{6}$$

where

T_e	=	electron temperature
e	=	electron charge
n	=	plasma density

The parameter T_e is used because electron mobility is higher than that of ions and therefore shielding is generally caused by the electrons. For an ionized gas to be called a plasma, it must be neutral enough that $n_i \approx n_e \approx n$, where n is a common density, n_i is ion density and n_e is the electron density. Collective behaviour requires that:

$$N_D >>> 1 \tag{7}$$

where N_D is the number of particles in the Debye sphere.

The collision frequency is also very important, if ω is the frequency of plasma oscillations and τ is the average time between collisions with the neutrals, it is necessary that $\omega\tau > 1$ for a gas to behave like plasma.

4.4 IONIZATION IN THE DUOPLASMATRON ION SOURCE

The gas to be ionized is introduced in the cathode side and interacts with the electrons emitted by the cathode. Ionization from the gaseous state is by electron impact. For ionization to occur, the energy of the electron impact ,E_e, should be greater than the energy needed to remove a bound electron.

$$E_e > e\phi_i \tag{8}$$

where ϕ_i is the first ionization potential of gas ionized.

Electron bombardment of the neutrals in the plasma is the most general method of increasing the plasma density. The contribution of the secondary electrons in the

ionization process is very small due to the high value of the self-collision (i.e. electron-electron collision) frequency by the secondary electrons causing their thermalization. Energetic electrons that go through into the second stage, contribute significant to the ionization process, because they are magnetically confined with minimum loses due to diffusion to the walls. Ionization by electron bombardment continues in the in the second stage.

In the case where protons are to be produced, ionization through electron bombardment of hydrogen is an important process to form a plasma. In the plasma state hydrogen can be the source of protons in several ways:

$$H_2 + e \Rightarrow H_2^+ + 2e$$

$$H_2 + e \Rightarrow H + H^+ + 2e$$

$$H_2^+ + e \Rightarrow H^+ + H + e$$

$$H + e \Rightarrow H^+ + 2e$$

$$H_2^+ + H_2 \Rightarrow H_3^+ + H$$

$$H_3^+ + e \Rightarrow H^+ + H_2 + e$$

The ion source is developed in such a way that all the processes that produce protons are enhanced.

4.5 ELECTROSTATIC DOUBLE LAYERS IN THE PLASMA

The electrostatic double layers influences electron emission by the cathode. These electrostatic double layers are caused by a decrease of electron mobility towards the anode, due to an increased magnetic field and/or pressure or due to geometric constrictions (i.e. constriction by the intermediate electrode). Electrostatic double layers can induce a rise in the electron temperature, which increases the chance to have full ionization of the gas and thus giving a high gas efficiency [**KIS65**]. There is a discharge mechanism in the double layer as a result of the potential jump. Double layers can also

act as a quasi cathode to supply the necessary extra electrons to produce the arc current at the anode.

4.6 EFFECT OF THE MAGNETIC FIELD AND THE ELECTROSTATIC POTENTIAL

The axial magnetic field is required to be maximum in the region between the IE and anode. Electrons in this region are extracted from the cathode plasma by the potential jump in the constriction sheath [**LEJ74I**]. The plasma sheath that results from Debye shielding on the electrode walls forms a potential barrier so that the mobile species, usually electrons, are confined electrostatically.

The Coulomb barrier adjusts itself to allow equal flux of both electrons and ions to reach the walls. At the anode sheath the electrons are reflected back whilst the positive ions are accelerated towards the anode. The electron mobility in the plasma is given by [**KIS65**]:

$$\mu_e = \left[(i\omega + \nu_m + \omega_c)m_e\right]^{-1}, \tag{9}$$

where

m_e = the electron mass and

ν_m = the elastic collision frequency of the electron in the plasma.

ω_c = The angular frequency at which the particles gyrate is called the cyclotron frequency, expressed as:

$$\omega_c = \frac{eB}{m} \tag{10}$$

The magnetic constriction influences the electron mobility, μ_e, and an excess of positive charges is created and thus a potential maximum appears between the IE and the anode where the magnetic field is maximum.

In a magnetic field, charged particles spirals around the magnetic field lines. The radius of this orbit is called the cyclotron radius or gyroradius (or Larmor radius) denoted ρ and it is given by:

$$\rho = \frac{mv_{\perp}}{qB} \tag{11}$$

where B is the magnetic field, m is the mass, q is the charge of particle and $v_{\perp}$ is the velocity component perpendicular to the magnetic field. The strong magnetic field confines the electrons over a very small radius and thus increases their path length, which leads to increased ionization.

As the ionization increases, the density of the plasma increases and the vibrations starts to appear in the plasma. Vibrations induce instability in the plasma and influence the output considerably. The frequencies thereof modulate the supply of positive ions through the plasma sheath. [**MAH58**].

4.7 ION EXTRACTION

In plasma ion sources, the plasma in the IE-anode region reaches the anode plate. High voltage is used to extract ions from the plasma. The applied field strength and the shape of the emitting surface influence the quality of the extracted beam. The plasma densities determine the shape of the emitting surface of plasma sources (**figure 4.2**) and hence influence the beam quality. The space charge limitation to the current that can be expected for charged particles accelerated by electric fields is given by:

$$j = \left(\frac{1}{9}\pi\right)\left(\frac{2q}{m_i}\right)^{1/2} \frac{U^{3/2}}{d^2} \tag{12}$$

where

j	=	current density
q	=	ion charge
m_i	=	ion mass
U	=	Extraction voltage in kV
d	=	acceleration gap

This is the Child-Langmuir Law [**BRO89**].

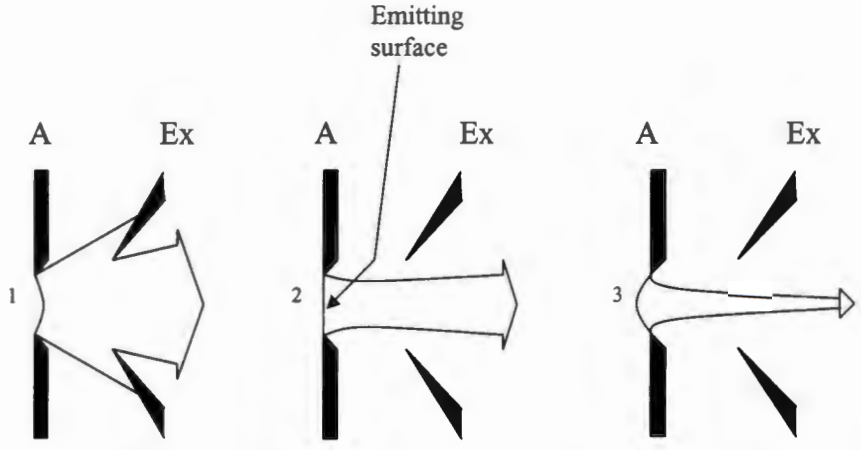

Figure 4.2: Schematic diagram showing how the shape of the emitting surface influence the beam quality with (1)-overdense plasma, (2)-medium dense, (3)- underdense plasma, A-anode and Ex-extraction electrode

CHAPTER 5

ION SOURCE CONSTRUCTION AND DEVELOPMENT

5.1 INTRODUCTION

The duoplasmatron ion source developed at *i*Themba LABS is in terms of the layout, similar to the source developed at the Pakistan Institute of Nuclear Science and Technology (PINSTECH) [**QAY94**], but since this source will be used for a different purpose, it was important to do some further development work to adjust the source to meet our requirements.

5.2 EXPERIMENTAL SETUP

The ion source is presently operated on a test stand. **Figure 5.1** shows the layout of the setup at *i*Themba LABS. The source is mounted vertically such that the beam is extracted downwards and then bends through 90^0 into the horizontal plane. One Faraday cup is placed just after the extraction from the ion source and another one just after the bending magnet. The bending magnet [**MAI02**] is also used as the mass analyzer. The first Faraday cup is operated with pneumatic actuators and the second one is in a static position in the beamline. The emittance measuring slit system is positioned just before the second Faraday cup. **Figure 5.2** shows the photograph of the test setup.

5.3 ION SOURCE DESCRIPTION

Figure 5.3 shows a diagram of the duoplasmatron ion source at *i*Themba LABS. The duoplasmatron ion source has an outside diameter of 80mm and a length of 100mm. The duoplasmatron has three electrodes, which are the cathode, intermediate electrode (IE) and the anode, with permanent ring magnets used to produce the axial magnetic field, B_z, in the source. Three magnets are positioned as a unit around the intermediate electrode and a single ring magnet at the cathode with electrical insulation material between the two sets of magnets.

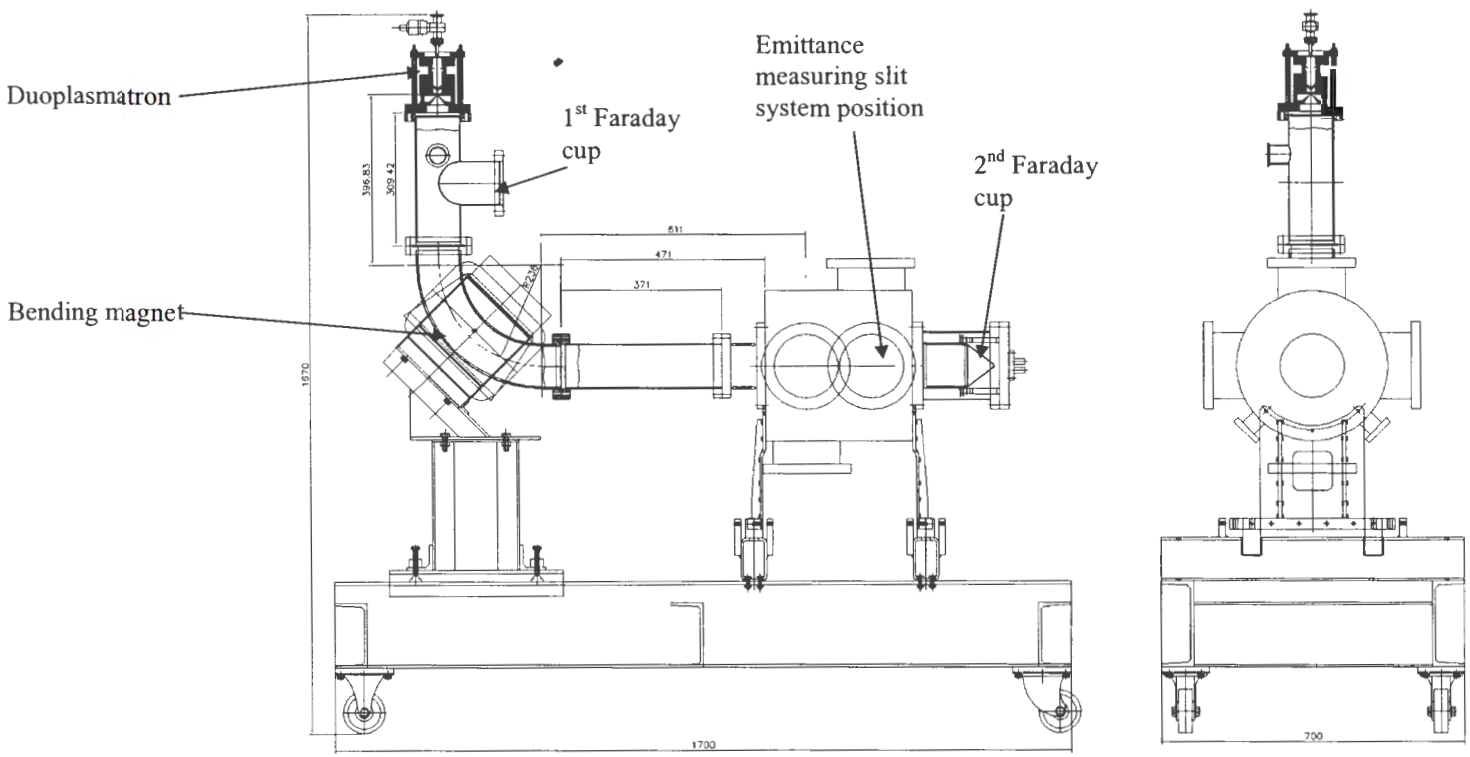

Figure 5.1: Side view elevation of the test stand with the source, bending magnet diagnostic equipment positions shown.

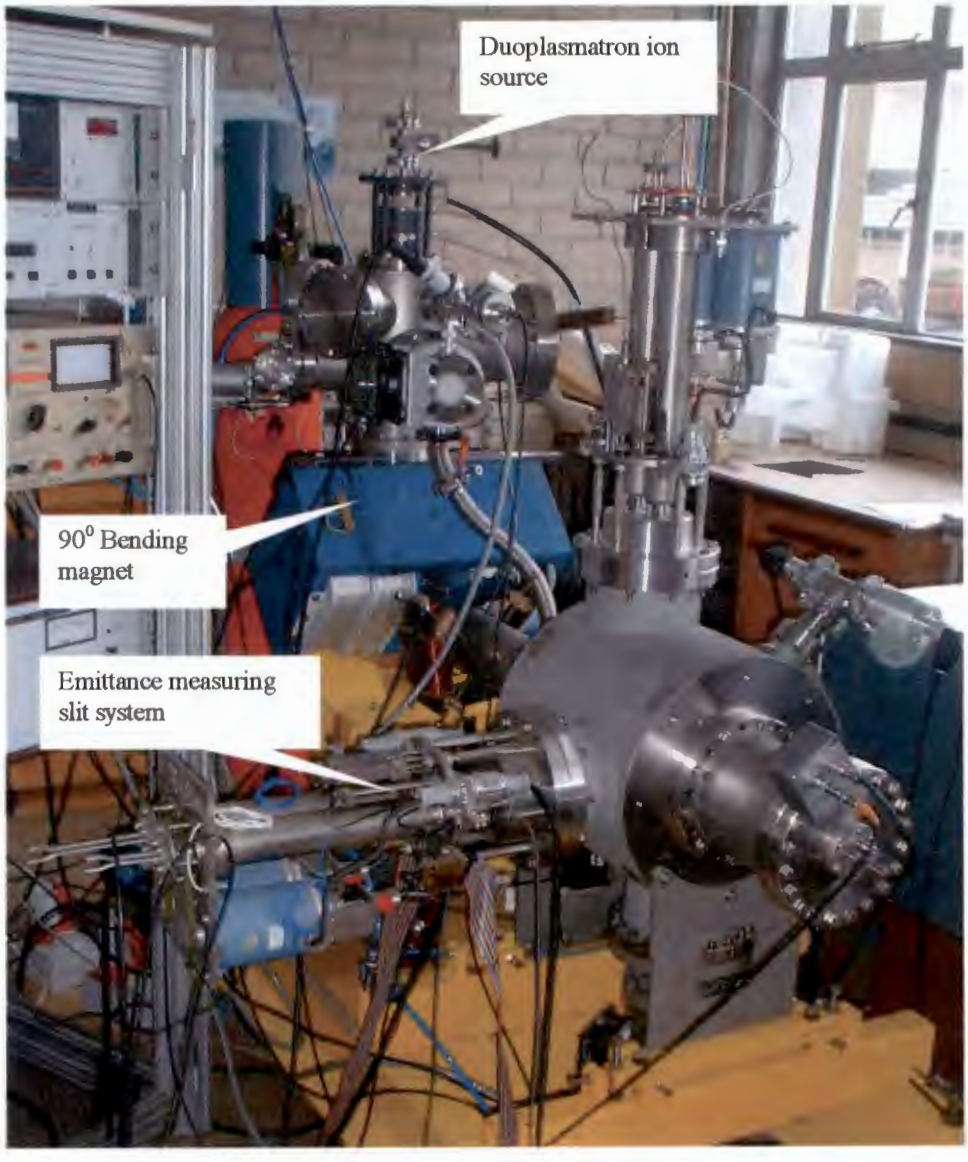

Figure 5.2: A photograph of the experimental setup showing the ion source mounted in a vertical position, the 90^0 bending magnet and the emittance measuring slit system.

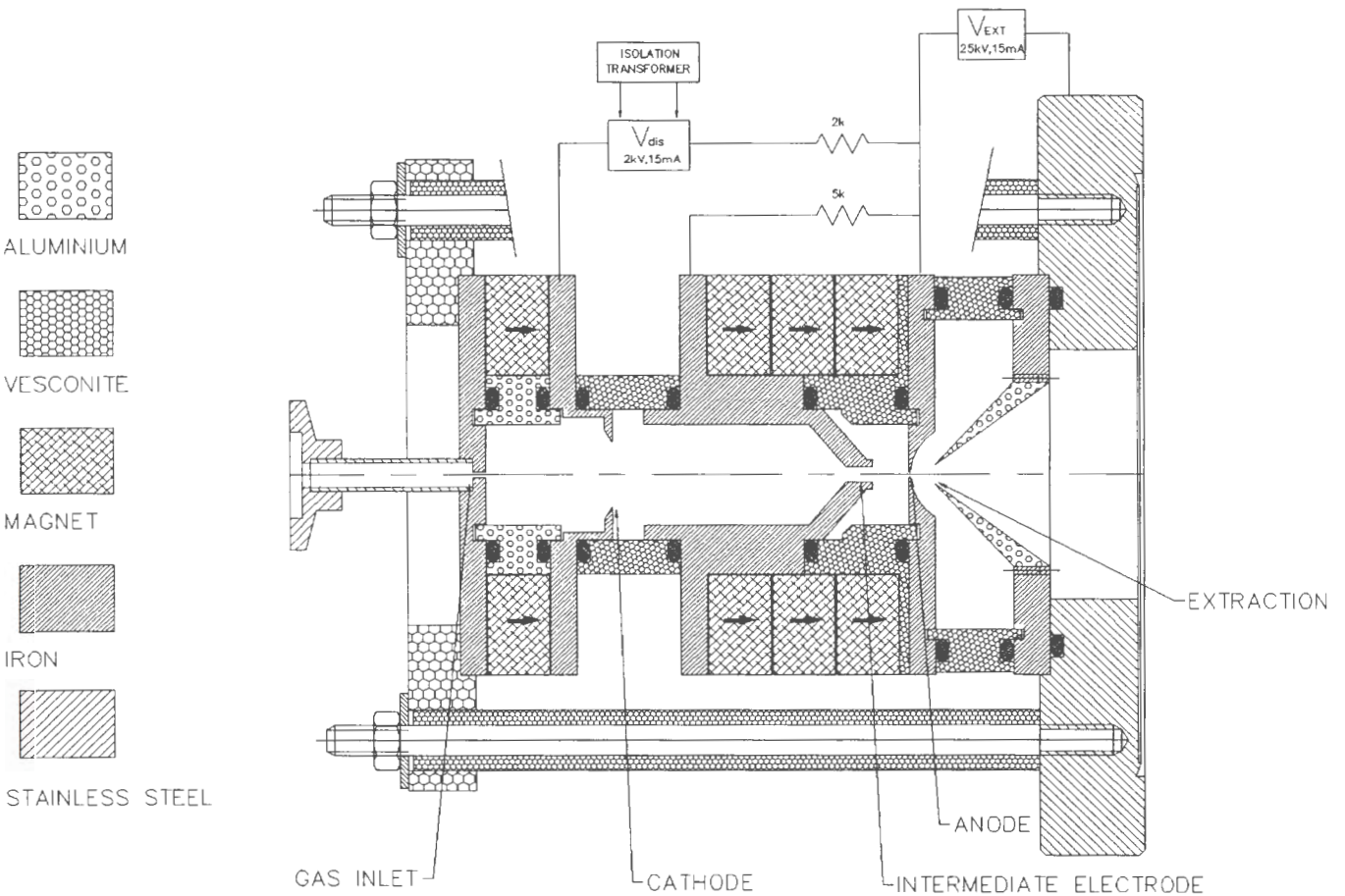

Figure 5.3: Diagram of the duoplasmatron ion source showing all the major components. The arrows on the magnets indicate the direction of magnetization.

5.4 MAJOR COMPONENTS OF THE DUOPLASMATRON ION SOURCE

Figure 5.4 shows a cross-section of the duoplasmatron ion source, with typical dimensions and its components. The main requirement is to build an ion source with good qualities in terms of beam intensity, stability, emittance and longer source lifetime. A general feature of source construction is to use materials with low sputtering probabilities, high melting points and exclude materials that are likely to introduce impurities in the gas discharge chamber.

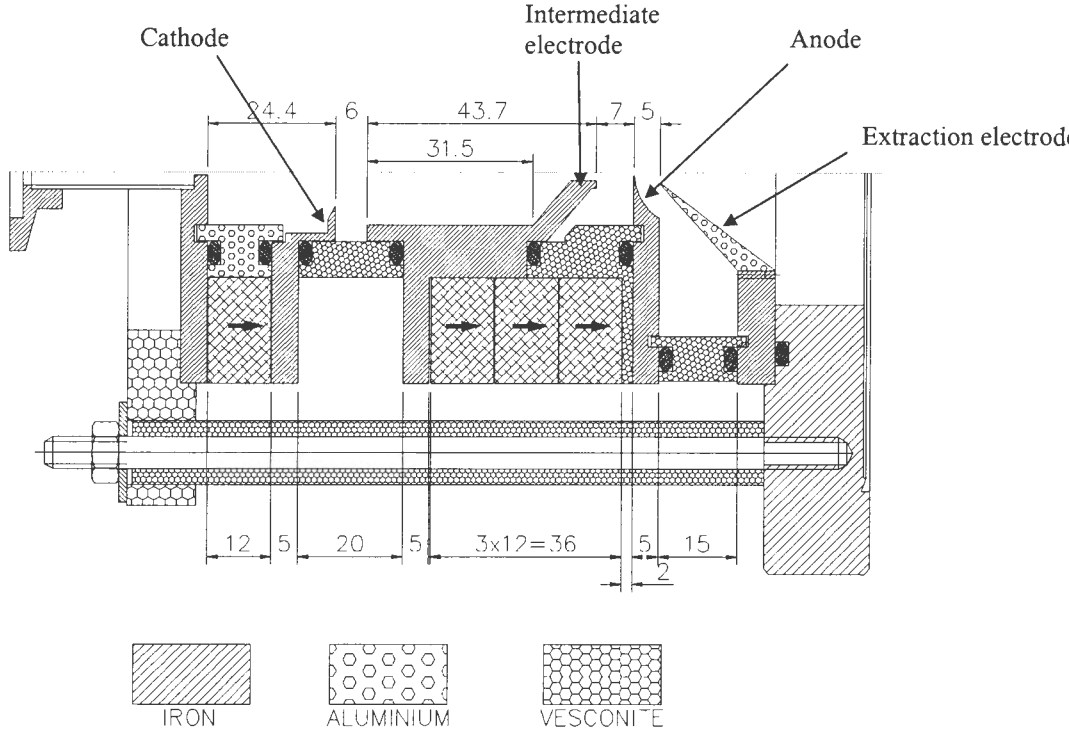

Figure 5.4: A cross-section of one half the duoplasmatron ion source along the axis of symmetry indicating the typical dimensions of the source.

5.4.1 HOLLOW CATHODE

The hollow cathode consists of two mild steel plates with an aluminum ring in the center. The cathode materials were chosen on the basis of their magnetic properties and arranged so as to give the highest magnetic field in the center and exit aperture of the hollow cathode. Desired cathode materials are materials with low sputtering probabilities that

will ensure an increased lifetime. The single ring magnet and geometry of the cathode provides the necessary field to ignite the arc.

5.4.2 INTERMEDIATE ELECTRODE (IE)

The IE is the electrode between the cathode and the anode. It is positively charged relative to the cathode and negatively charged with respect to the anode. The IE is conical towards the exit aperture. This is done to constrict the plasma as it flows towards the anode through the IE exit aperture and it influences the distribution of the field at the anode side, because of its magnetic properties.

5.4.3 ANODE

The anode is a flat mild steel plate and has a small tapered aperture at the center. Tapered aperture is bigger at the extraction side and allows the plasma to expand and cool before the final ion extraction. The size of the anode aperture can influence the ion yield from the source.

5.4.4 EXTRACTION ELECTRODE

The extraction electrode is made from aluminum and conical in shape. It extracts and accelerates the ions from the source. The positioning of the extraction electrode relative to the anode can be varied to obtain the optimum beam current.

5.4.5 RING MAGNETS

Ferromagnetic ring magnets provide the necessary magnetic field in the ion source. A total of four ring magnets are used in the source, one ring at the cathode and a set of three rings around the intermediate electrode. The dimensions of the ring magnets are: 40 mm inside diameter (ID) by 80 mm outer diameter (OD) by 12 mm wide.

5.4.6 POWER SUPPLIES

A RHVS 2-1000 power supply was used as an arc power supply. The voltage and current are adjustable over the entire range from zero to the maximum voltage via ten-turn potentiometers with lockable dials. The power supply has the input voltage of $220 \pm 10\%$

VAC, output voltage of 2kVdc, output current of 500mA reversible polarity and digital voltage and current meters, accurate to 1% [**RHVS 2500 series manual**]. A HNCs 120 000 – 5 Reversible power supply was used as an extraction power supply with the maximum output voltage of 120kV and a maximum out put current of 5mA. [**HNC manual**]

5.5 PHYSICAL OPERATING PARAMETERS AND RANGES OF VARIATION

Physical changes had to be done on the operating parameters during the development and optimization process. Below is the list of parameters that were changed and the ranges over which the changes were made. The results obtained will be presented in the next chapter.

Geometric parameters:

D	: diameter of the IE opening	3 - 5mm
d	: diameter of the anode aperture	0.5 - 1.2mm
l	: anode-extractor separation	5 - 10mm
L	: IE-anode separation	3 - 15mm

Electrical parameters:

V_e	: extraction voltage	12 - 20 kV
V_a	: arc voltage	60 - 80V
I_A	: arc current	20 - 100mA

Gas flow 1.5 - 2.5cm^3/min

5.6 MAGNETIC AND ELECTRIC FIELD CALCULATIONS

Due to the small dimensions of the source it was not possible to use probes in the source to measure any of the magnetic or electric field distributions in the source. A commercial computer program from Vector Fields, OPERA-3d, was used to calculate, simulate and optimize the fields in the duoplasmatron ion source. This software package consists of a pre and post processor with optional analysis modules for different types of solutions in

numerical field analysis. The TOSCA module computes magnetostatic and electrostatic fields in three dimensions and was used for all calculations and simulations in this dissertation. It uses a discrete finite element model to solve partial differential equations governing the behaviour of electromagnetic fields **[http://www.vector-fields.co.uk/opera3d.html]**.

Before performing the actual calculations on the source, the accuracy of the calculated results as well as the magnetic material characteristics were determined by comparing the field distribution results of a geometry that also permitted physical measurements. The geometry included an assembly of three ring magnets with dimensions: 40 mm inside diameter (ID) by 80 mm outer diameter (OD) by 12 mm wide and two steel plates, one at each end of the assembly (**figure 5.4**). Each plate has a hole to allow the probe through the center of the assembly. The axial magnetic field component was measured along the axis of the geometry and compared to the results of the calculations from OPERA-3D (see **figure 5.5**), where material properties were adjusted until the calculations represented the measured values. The results provided material characteristics that can be used with confidence in the field analysis calculations for the source.

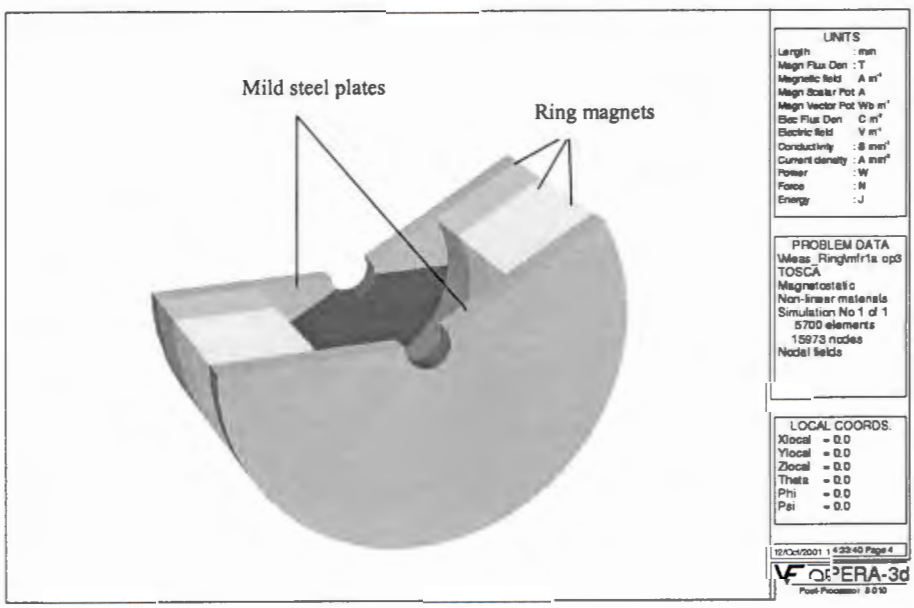

Figure 5.4: A portion of the test geometry consisting of three magnets and two mild steel plates. Probes were inserted through the openings on the steel plates.

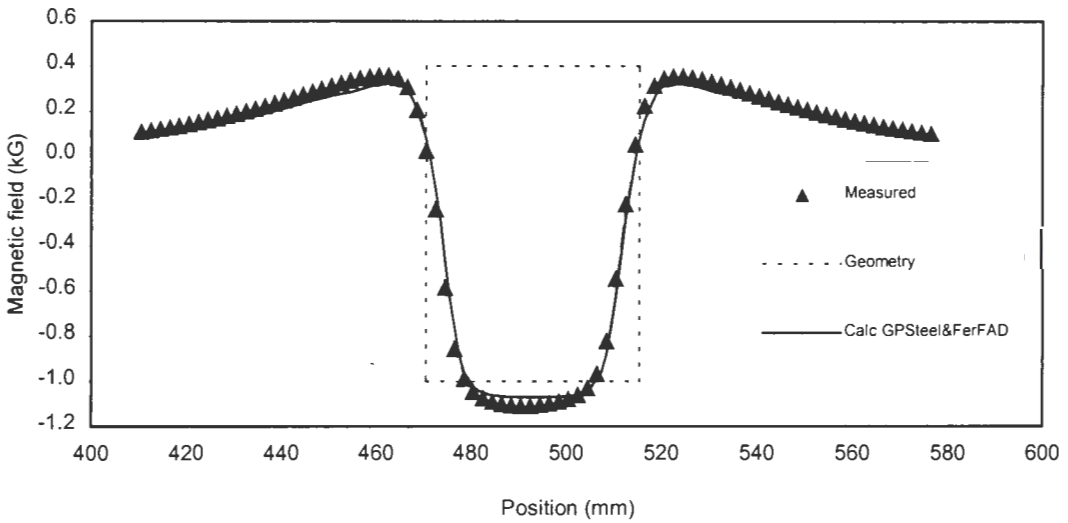

Figure 5.5: Graph showing the comparison between the measured and calculated axial magnetic field obtained along the axis of the magnet set-up. It provides a method to establish the magnetic material characteristics, which can be used with confidence in the calculations for the duoplasmatron ion source.

5.6.1 AXIAL MAGNETIC FIELD PROFILE IN THE ION SOURCE

A three-dimensional finite element simulation of the geometry of the electrodes (see **figure 5.6**) was made and was used for the calculations and plotting of the fields. The magnetic field distribution in the source was calculated using the computer code OPERA-3d as shown in **figure 5.7 and 5.8**. The horizontal z-axis in **figure 5.7** corresponds to the actual length of the ion source with the extreme outer surface of the cathode at $z = 0$ mm. The maximum magnetic field is in the region corresponding to the IE-anode region. The region inside the IE is magnetic field free. This is the desired distribution for enhanced electron confinement. The field density distribution is shown in **figure 5.8**, the white colour represents electrodes, purple and orange shows ring magnets around the IE and the cathode whilst the rest of the colours represent the magnetic field distribution in the free space in the ion source. In this space, the maroon shows the region with the most intense magnetic whilst blue shows the lowest field density region in the source. The arrows show the direction of the field, both in materials and free space.

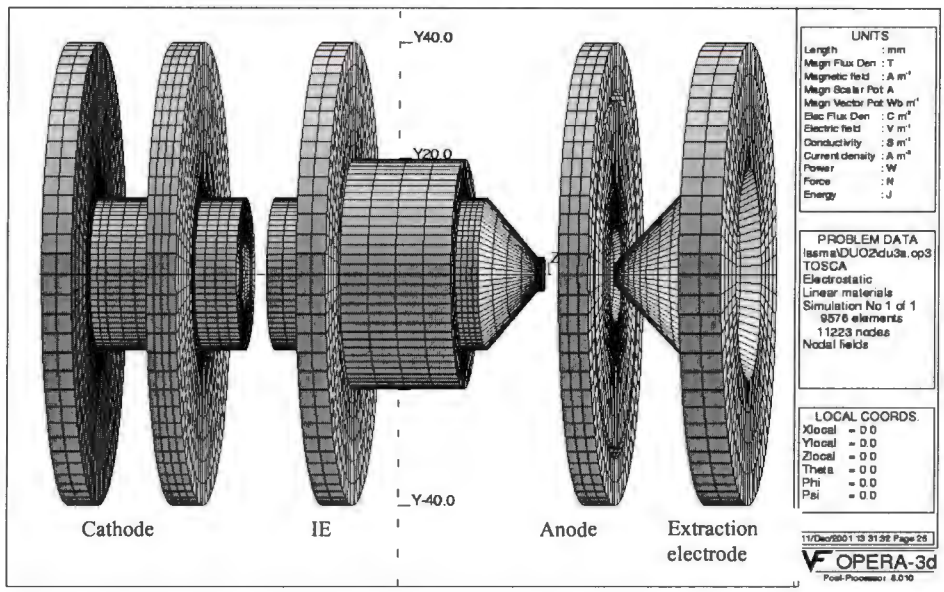

Figure 5.6: A 3d-finite element simulation of the mild steel electrodes using OPERA-3d with the TOSCA module. The magnets are not shown.

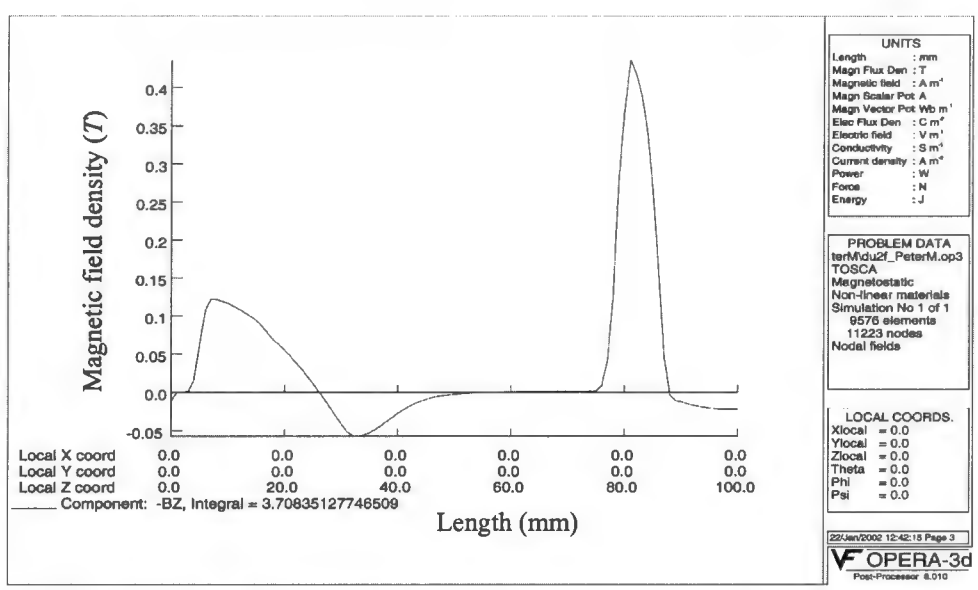

Figure 5.7: Profile of the calculated axial magnetic field, B_z, profile as a function of z along the axis of the source.

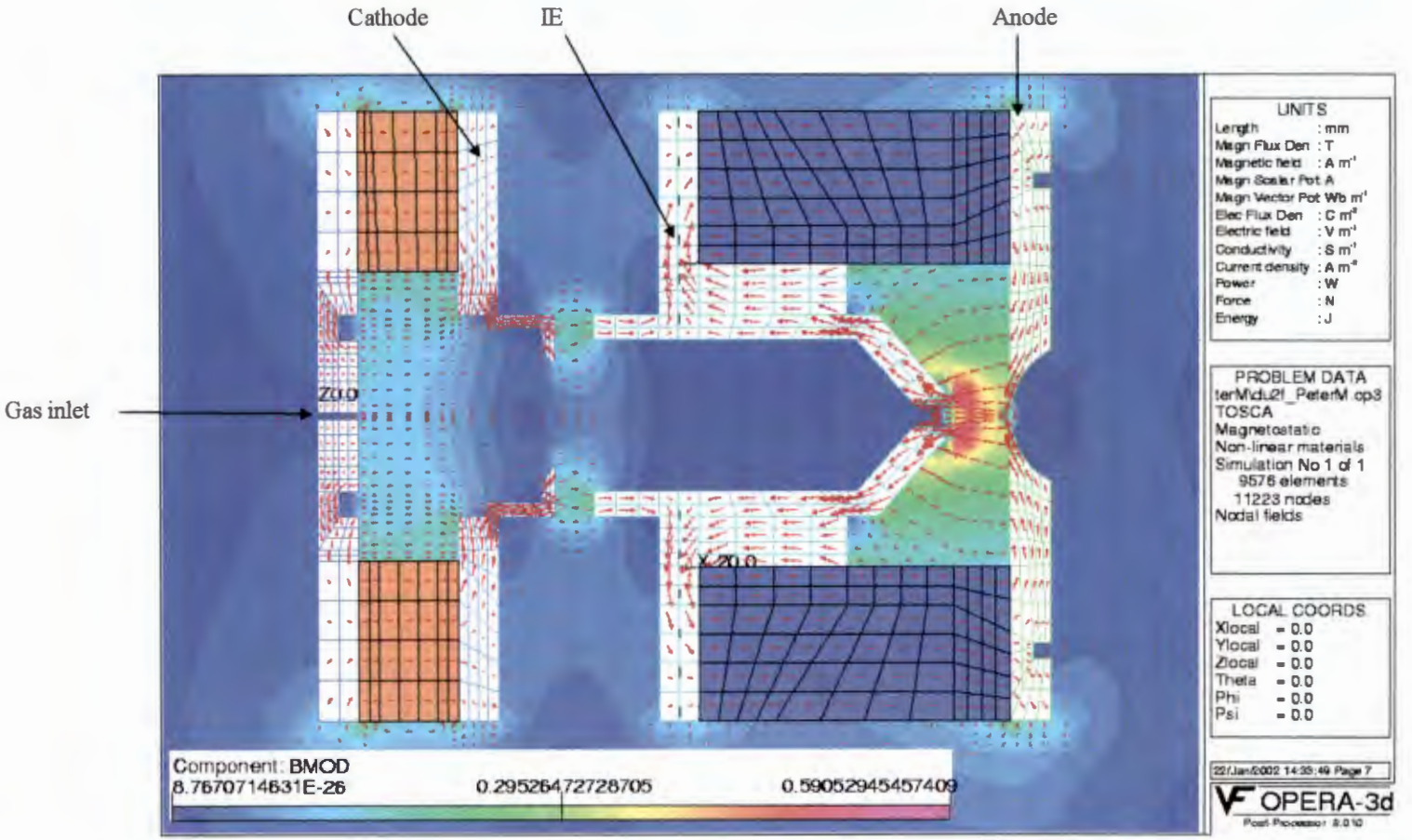

Figure 5.8: The calculated magnetic field density distribution shown on a section of the duoplasmatron ion source. The electrodes are shown in white, purple and orange shows the ring magnets around the IE and the cathode, whilst the rest of the colours represent the free space in the source. In this space, the maroon shows the region with the most intense magnetic field, whilst blue shows the lowest field density region on the colour scale. The arrows show the direction of the field.

5.6.2 ELECTRIC FIELD AND ELECTROSTATIC POTENTIAL PROFILES IN THE ION SOURCE

Figure 5.9 shows the calculated electric field profile along the symmetry axis of the source. The computer program OPERA-3d with the TOSCA module was used to do the calculation.

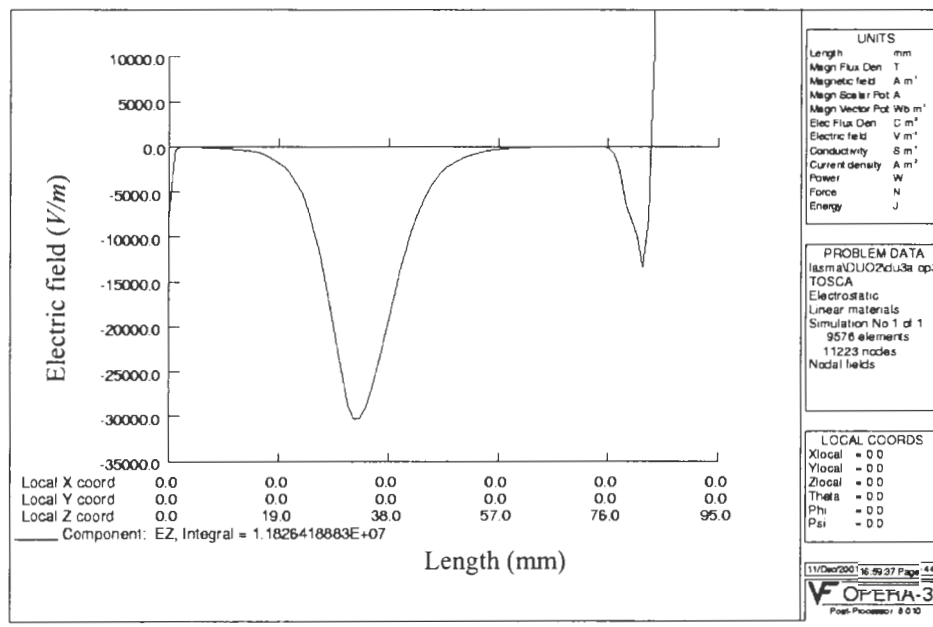

Figure 5.9: The calculated electric field strength profile along the symmetry axis of the ion source.

The graph peak with the maximum negative field value corresponds to the spacing between the cold cathode and the IE. The other negative electric field peak corresponds to the area between the IE and the anode. The twp regions along the z-axis where there is no electric field, corresponds to the region inside the cathode and to that inside the IE. The electric field ensures electron flow from the cathode to the IE and from the IE to the anode.

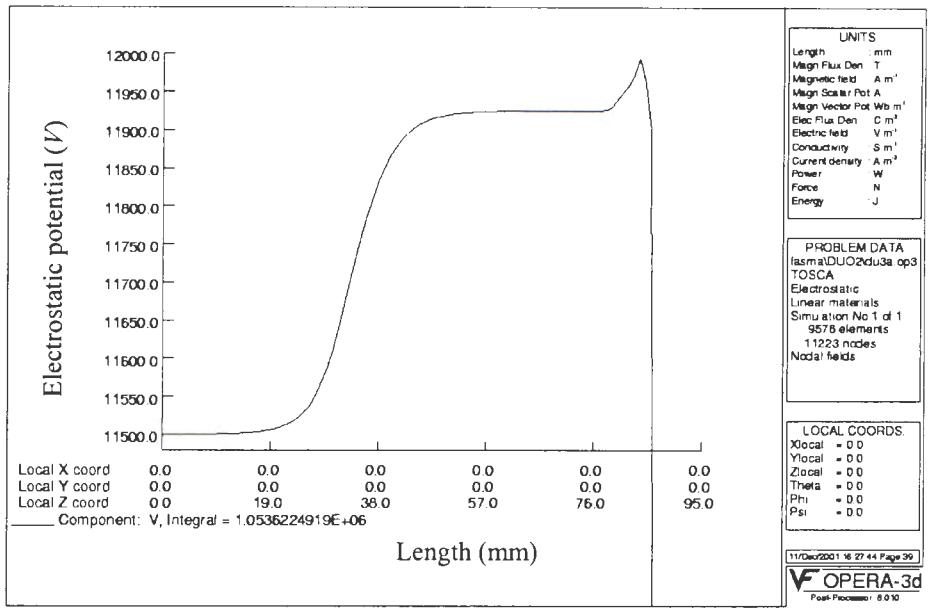

Figure 5.10: Calculated potential distribution along the z-axis in the source. The potential at the extraction components is not shown.

Figure 5.10 shows the calculated potential distribution along the z-axis. The first region where the graph appears flat corresponds to the cathode region. The highest potential difference is in the region corresponding to the spacing between the cathode and the IE. The second plateau on the graph corresponds to the region inside the IE. The second region where the highest potential difference appears corresponds to the region starting from the IE aperture to the anode. The sharp drop-off is the region outside the anode that was not included in the calculation of this graph. This kind of potential distribution is desired to have the electrons flowing from the cathode in the direction of the anode.

4.6.3 SIMULATION OF ELECTRON TRAJECTORIES IN THE DUOPLASMATRON ION SOURCE

The calculated magnetic and electric fields for the operating conditions were combined for the tracking of electron trajectories in the different plasma regions of the douplasmatron ion source, but plasma and space-charge effects were not taken into account. The calculated electron trajectories with an initial energy of 10 eV from the tip of the cathode, but with different divergences are shown in **figure 5.11**, superimposed on

a wire-frame geometry of the source. With all the mentioned pre-conditions, it resulted that all the electrons with an initial divergence between 26 and 35 degrees relative the z-axis, will proceed through both the IE-plasma region and the IE-aperture into the important IE-A region near the anode

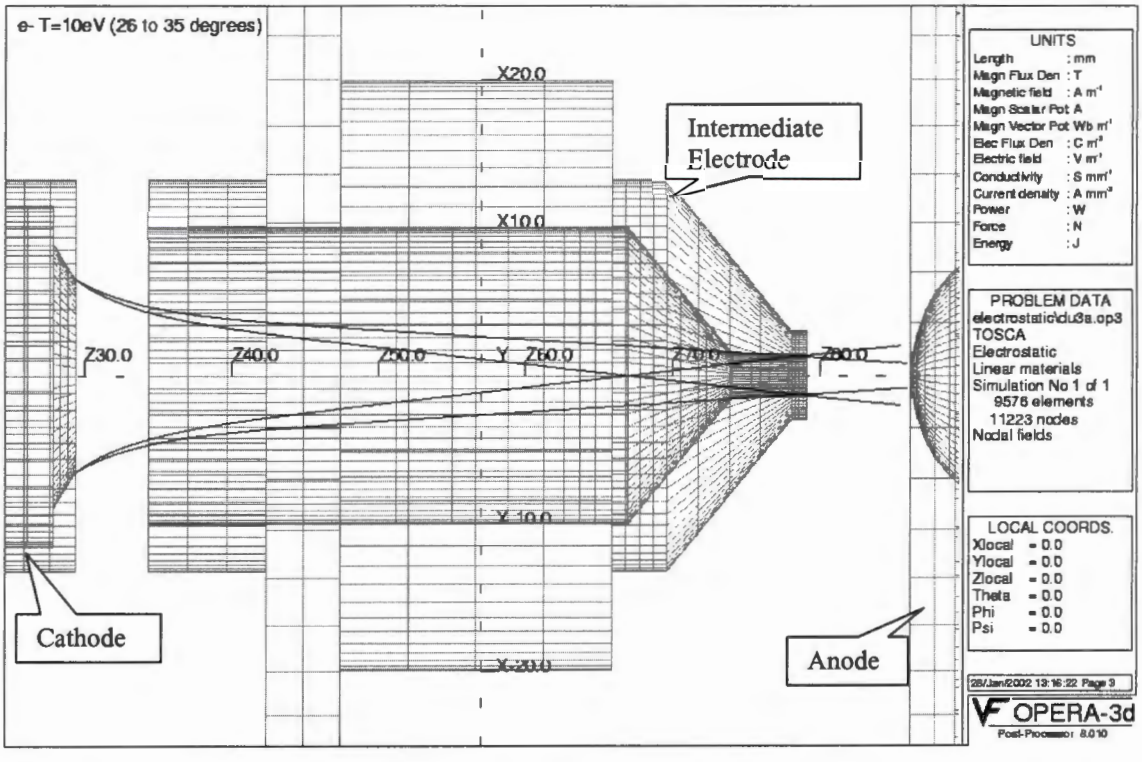

Figure 5.11: The calculated trajectories of electrons, all with initial energy of 10eV, but with different divergences, starting from the cathode exit and space charge or plasma effects were not taken into account in the calculation.

CHAPTER 6

OPTIMIZATION OF THE COLD CATHODE DUOPLASMATRON ION SOURCE

6.1 INTRODUCTION

The influence of the different operating parameters of the source on the beam quality and intensity were investigated to determine the optimum operating conditions for the maximum beam output from the source. Different operating parameters of the duoplasmatron ion source were optimized to create a condition that leads to an overall improvement in the source performance.

6.2 INFLUENCE OF OPERATING PARAMETERS ON THE BEAM CURRENT

The beam current from the source can be influenced by the geometry and discharge parameters like, arc current, magnetic field and the pressure. As a way of optimizing the ion source, four to five changes where made to one parameter whilst keeping the other parameters constant. The optimum operating conditions were determined by graphically plotting the measured beam currents as a function of the different parameters.

6.2.1 INFLUENCE OF THE ANODE APERTURE DIAMETER

Five anode plates with different aperture diameters were manufactured and tested in the ion source. The measured extracted beam current is shown in **figure 6.1** as a function of the different aperture diameters and keeping all other relevant parameters constant. The ion beam output through the anode aperture is to a larger extend dependent on the anode aperture diameter. The linear dependence of the current density on the anode aperture opening in the aperture ranges from 0.5mm to 0.8mm. The beam current I_b, as a function of the radius r of the aperture has in this region the relationship:

$$I_b \propto \mathrm{r} \tag{13}$$

This implies that the current density drops off inversely proportional to the radius as a

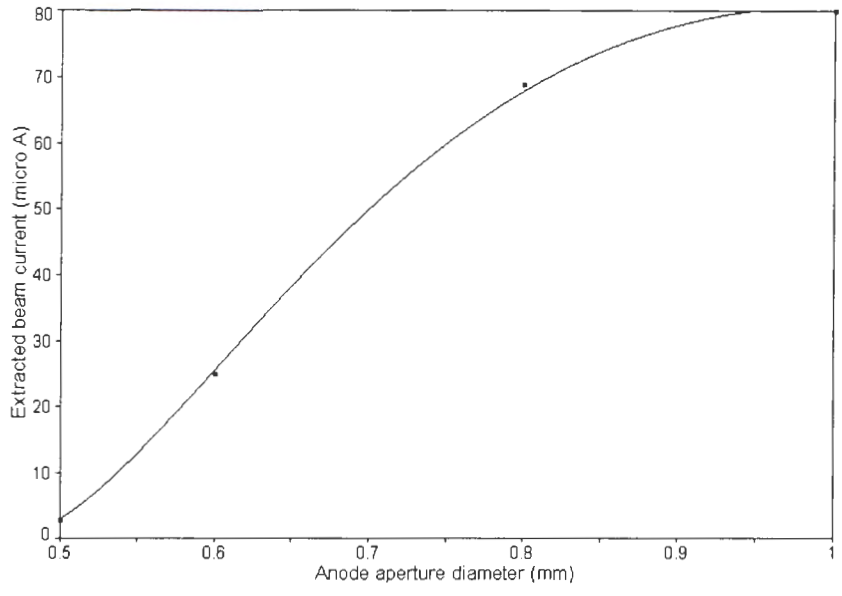

Figure 6.1: Effect of the anode aperture diameter on the extracted beam current.

first approximation. The optimum current I_b is obtained at an aperture diameter of 1mm. The flattening of the graph for the aperture diameter above 0.8mm is not fully understood yet and is probably due to the limited aperture of the extraction electrode and beam blow-up due to space charge forces. The source was unstable with a 2mm aperture diameter, which could be caused by the whole plasma flowing through the anode aperture.

High currents shown in the plot are as a result of having an expansion cup on the anode, which was not used in the other measurements.

6.2.2 INFLUENCE OF THE IE-ANODE SEPARATION DISTANCE

In the IE-anode plasma region it is important to adjust the geometry to match or coincide with the desired configuration of both the magnetic and electrostatic potential distributions to give a higher beam current. To avoid recombination of secondary electrons and ions, it is important to have the anode position just at the end of the magnetic bottle. Magnetic confinement of energetic primary electrons leads to the rise in the electron temperature T_e, which then increases the ionization probability. When the IE-anode separation distance is too big, possibilities of plasma cooling increases and may

lead to reduced ionization probabilities in the region. **Figure 6.2** shows how the beam current changes as the IE-anode gap changes.

The separation distance between the anode and the IE determines the length of the anode column and this influences the axial electrostatic potential distribution along the discharge. As the anode-IE separation distance increases, the beam current drops. This can be attributed to the loss of ions due to recombination in that region. From **figure 6.2**, the maximum current was recorded for a separation of 6mm between the anode and the IE.

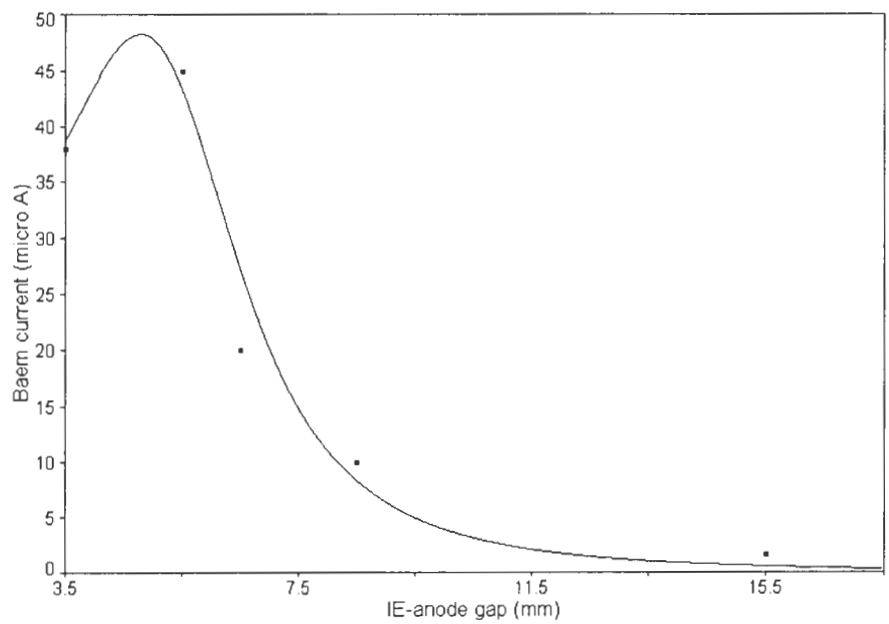

Figure 6.2: Effect of the IE-anode gap on the measured extracted beam current.

6.2.3 INFLUENCE OF THE IE APERTURE DIAMETER

Due to constrictions of the plasma discharge, one or more double layers are generated along the plasma column, separating region of different neutral pressure and plasma density [**ANG83**]. The IE acts to constrict the plasma and this results in the formation of an electrostatic layer [**KIS65**]. This creates a potential discontinuity at the cathode side of the IE. A double layer in the plasma acts as a quasi cathode to supply the electrons necessary for ionization in the second stage discharge. In **figure 6.3**, there is a decrease in the beam current as the IE aperture diameter increases to higher than 3mm, because it is

in effect a decrease in the constriction, which makes the double layer disappear and thus no longer have the extra electrons available in the second stage. It was observed that with a 3.5mm diameter, the source was stable and could operate at lower gas pressure. When the gas pressure in the beam line was lowered to 1.5×10^{-5} mbar and the arc current raised to 80mA, a 60μA proton beam was extracted.

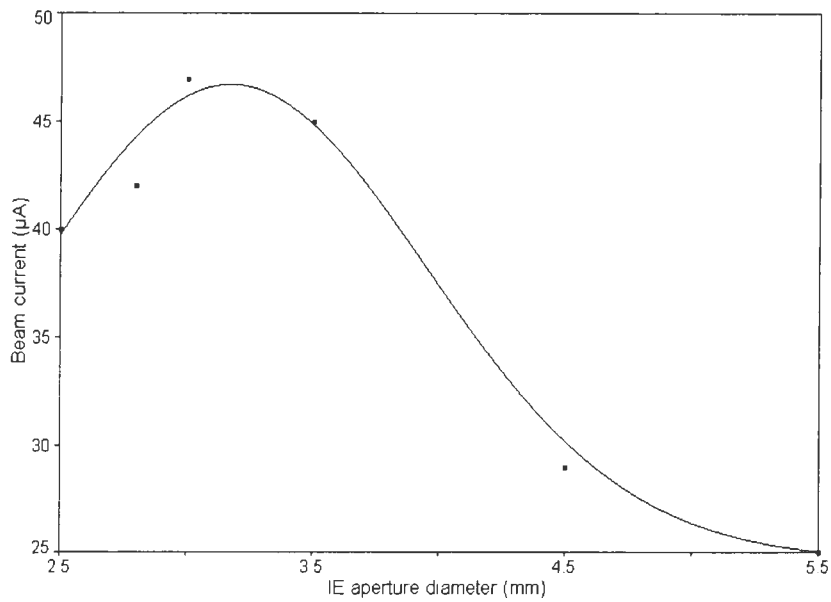

Figure 6. 3: Graph showing how the IE aperture diameter influence the measured beam current.

6.2.4 INFLUENCE OF THE ARC CURRENT

During the experiment, the gas pressure was set such that the discharge continued even at the lowest arc current. The extraction voltage and other parameters were kept constant. Measurements were made for both the total and analyzed beams. The beam current shown in **figure 6.4a and 6.4b** respectively is directly proportional to the arc-current. It is also evident that as the arc current increases, there is a change from the normal arc mode to arc starvation mode. The neutral density inside the arc column decreases as the arc current is increased, which is due to the high ionization efficiency and leads to the total depletion of the gas in the source as a result of the high arc current.

At higher gas pressure, high arc currents can be applied. But due to the nature of the insulator and other materials in the source this is better done for only short periods. An

arc current of about 100mA should not be exceeded during operation because it may damage the source components.

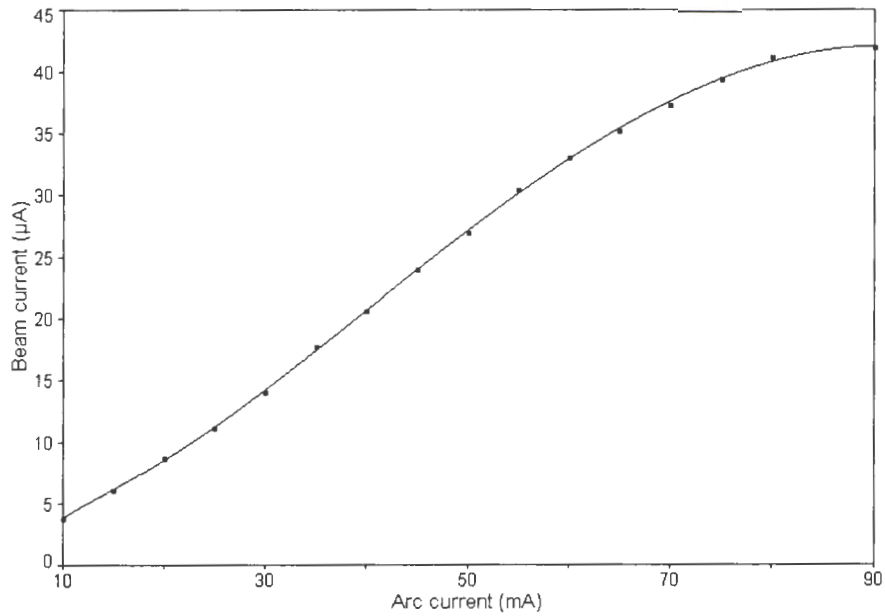

Figure 6.4a: Dependence of the analyzed proton beam current on the arc current

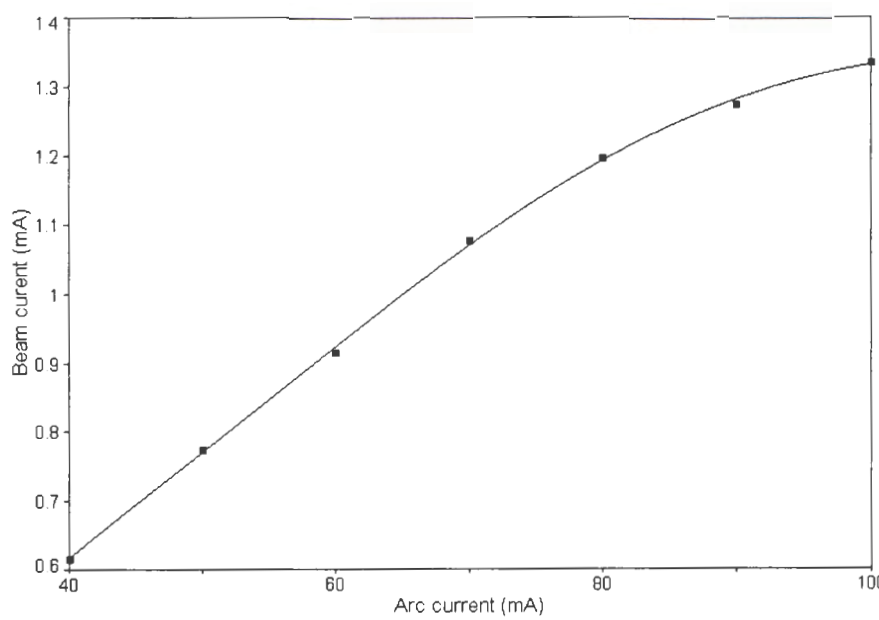

Figure 6. 4b: Influence of the arc current on the total beam current

6.2.5 INFLUENCE OF THE EXTRACTION VOLTAGE

The field created by the extraction voltage accelerates the positive particles out of the source as a beam. **Figure 6.5a and 6.5b** shows how the extraction voltage influences the beam current. The beam current was measured before and after mass separation.

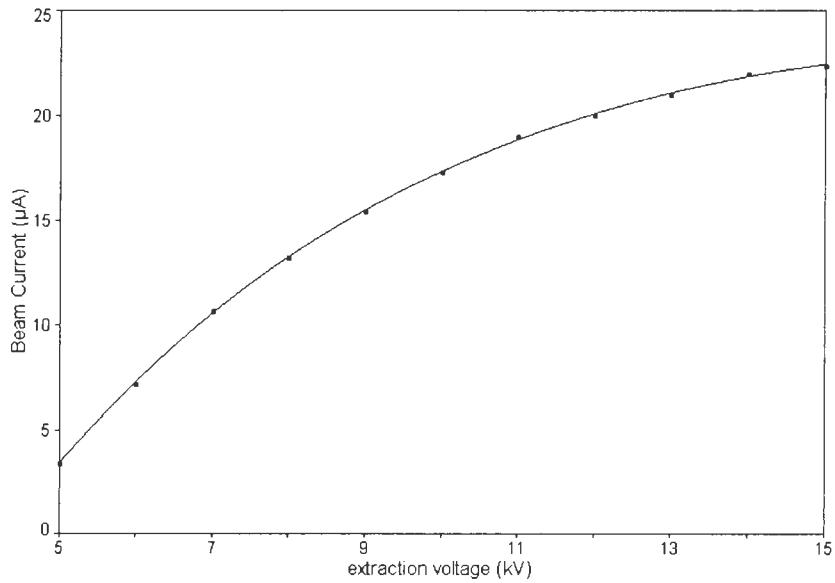

Figure 6.5a: Response of the analyzed proton beam current to changes in the extraction voltage

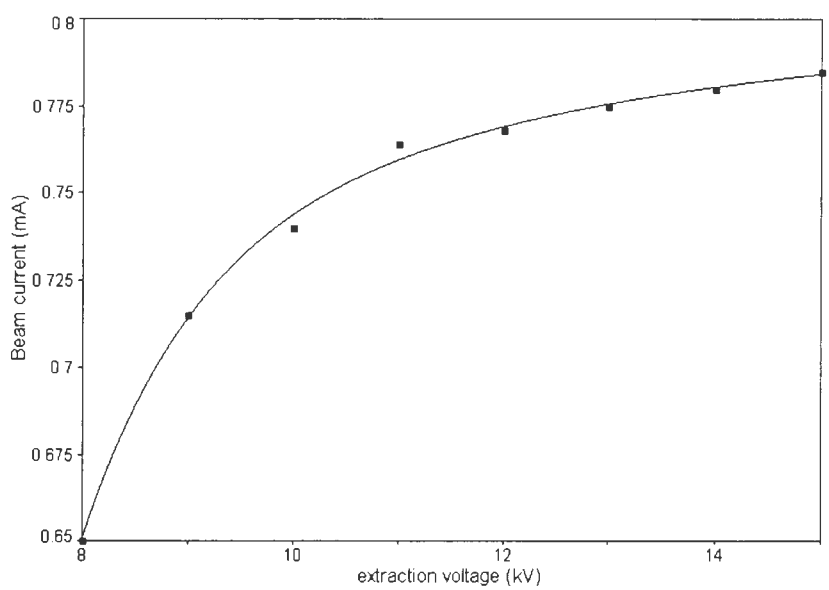

Figure 6.5b: Response of the total beam current to changes in the extraction voltage

From the graphs it can be seen that as the extraction voltage increases, the extracted beam current also increase (i.e. more protons are accelerated out of the source). According to the Child-Langmiur law, the extracted ion beam current exhibits the dependence:

$$I_b \propto U^{3/2} \tag{14}$$

where U is the extraction voltage and I_b beam current. From observation there is a possibility that space charge effects might be a reason for the deviation seen on the graph.

6.2.6 INFLUENCE OF THE GAS PRESSURE

It was not possible to measure the pressure in the source because of the small dimensions of the source, but it was measured in the beamline. It is assumed that the pressure in the source will vary in the same manner as the pressure in the beamline. As the beam current measurements were made, the pressure was the only parameter that was varied. An almost similar trend was observed in both the total beam (before mass separation) and the analyzed beam (after mass separation) (**figure 6.6a and 6.6b**).

Due to the fact that ion generation is proportional to the pressure, there will be a minimum pressure at which the arc will be unstable or extinguish [**GUT49**]. A gas pressure of 1.5×10^{-5} mbar seemed to be the minimum pressure at which the arc functions properly.

At lower gas pressures, there is a higher probability for the primary electrons to reach the second discharge stage leading to improved ionization possibilities and thus higher beam current. This is due to the reduced probability of ion losses as a result of recombination. It should also be noted that at too low gas pressure the arc mode changes to starvation.

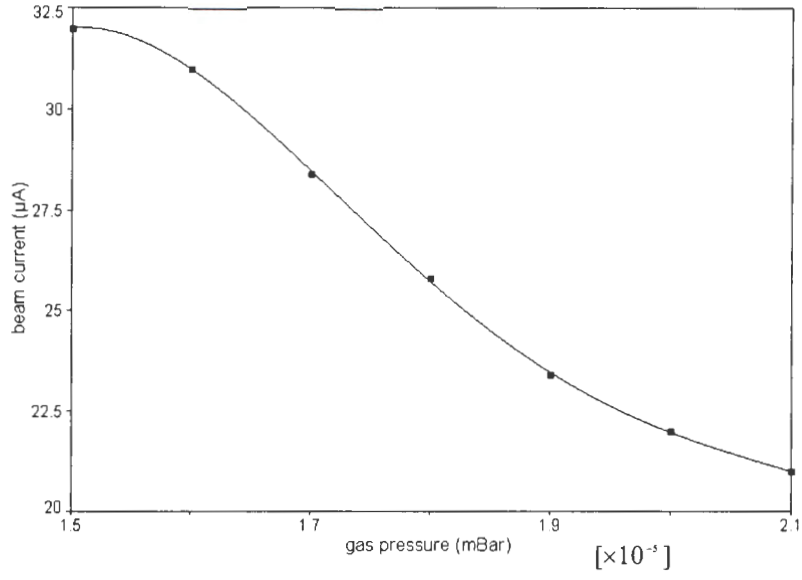

Figure 6.6a: The relationship between analyzed proton beam current and the pressure in the beamline.

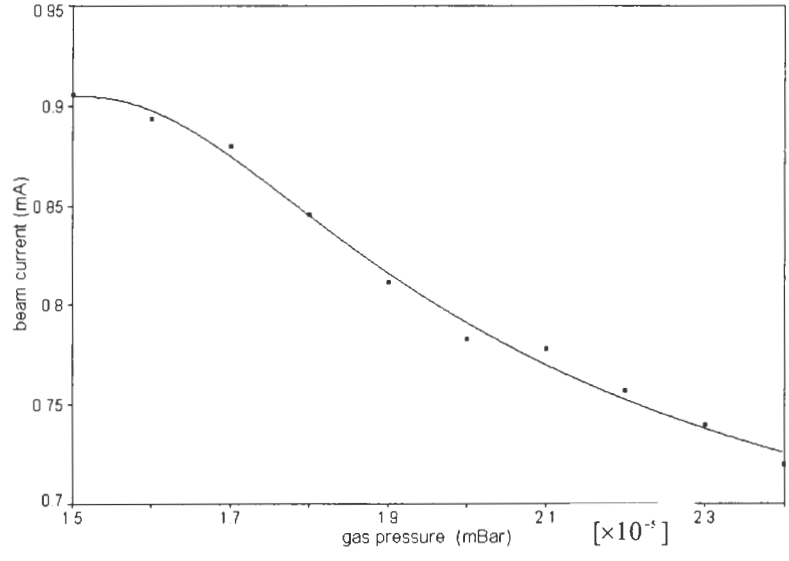

Figure 6.6b: The relationship between total beam current and the gas pressure in the beamline.

6.3 THE INFLUENCE OF A Cu PLATE FIXED ON THE ANODE

A 1mm thick copper plate was fixed on the anode in the IE-side and a 30% increase in the H^+ beam current was recorded with this copper insert. The anode outlet was now effectively moved backwards to a region with a higher magnetic field as shown in **figure 6.7** where the ionization probability is higher.

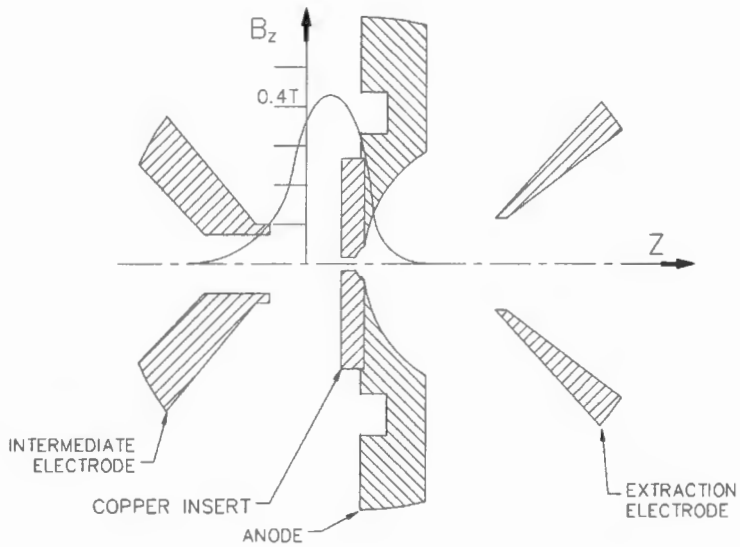

Figure 6.7: Diagram showing the location of the magnetic field peak along the z-axis with the copper insert fixed on the anode.

6.4. PERCENTAGE COMPOSITION OF THE BEAM

From the total hydrogen beam extracted from the source, it was found by mass analysis that the beam on average consists of:

H^+: ≤15%

H_2^+: ≤30%

H_3^+ ≥55%

6.5 PRODUCTION OF OTHER IONS

6.5.1 INTRODUCTION

Due to the short containment time of this ion source, it would not be easy to produce multiply charged ions. According to [**ANG83**], the highest charge states of Xenon can be reached using very narrow IE apertures and high magnetic fields. The production of other single charged ions with this type of a duoplasmatron ion source, other than H^+ has been explored.

6.5.2 PRODUCTION OF He^+ ION BEAM

Duoplasmatron ion sources can also be used for the production of He^+ ions. Table 1 presents the results obtain during operation with helium gas.

Table 1: *Results obtained during operation with helium gas*

Ion	Extraction Voltage	Beam Current
He^+	12kV	93μA
He^+	10kV	86μA
He^{++}	12kV	1μA
He^{++}	10kV	0.8μA

The above measurements were made at a gas pressure of 2.0×10^{-5} mbar in the beamline. At a gas pressure of 1.0×10^{-5}mbar there was an improvement in the He^{++} current.

Table 1 shows that the duoplasmatron can be a good source for He^+ ions with a current of 93μA. For He^{++} ions the current is very low but it can still be useable in some cases.

CHAPTER 7

THE EMITTANCE OF THE DUOPLASMATRON ION SOURCE

7.1 INTRODUCTION

Ions leave the duoplasmatron ion source from any point in the exit aperture, with a spread in their initial velocities, both in terms of magnitude and direction, which is caused by the high temperatures inside the ion source and the consequent collisions between the particles. The velocity spread in the beam may be considerably larger than what would be expected from the temperature alone, since temperature fluctuations in the plasma, plasma instabilities and non-linear forces due to external fields and space charge lead to an increase in the velocity spread. A beam from an ion source has therefore, in addition to its height and width, an energy spread and angular divergence in both the horizontal and vertical directions. Different permutations of these parameters define the quality of the beam extracted from an ion source.

7.2 BEAM EMITTANCE

Emittance provides a quantitave basis for describing the quality of a beam. A beam propagating a direction has two symmetry planes in which the motion of each individual particle is defined by the three space coordinates (x, y, z) and the three momentum coordinates (p_x, p_y, p_z) at a given instant in time. Particle trajectories in most beamlines have very small transverse velocity components and the variation in the direction of propagation is also negligible. The divergence angles of a beam propagated along the z-axis can be approximated by the tangent values $x' = dx/dz$ and $y' = dy/dz$, instead of the transverse linear momenta, $d(mx)/dt$ and $d(my)/dt$, divided by the momentum in the direction of propagation. Commonly used two-dimensional emittance definitions therefore relate the patterns that particle trajectories independently occupy in the (x, x')

and (y, y') planes. The combination of these planes forms a four dimensional space referred to as phase space.

Two different conventions are in use to quantify emittance. Either the area occupied by the beam in phase space, in units of mm mrad or of m rad, or the area divided by π, can be used as definition of emittance. The latter convention results from the fact that beams frequently occupy regions of elliptical shape in phase space and that the extent of one semi-axis of the ellipse can directly be deduced when the emittance and the other semi-axis are known. However, the majority of publications on this subject do not explicitly mention which of these conventions is being used.

A third convention, which retains the advantages of the second convention, will be used in this thesis. The emittance is defined as the area in the phase space, but π is written as a distinct factor and forms part of the unit of emittance. The unit of emittance with this method is thus π mm mrad.

The confusion brought about by these three conventions is further increased when statistical distributions in phase space and the root mean square, *rms*, values of emittance are being used. The rms emittance is defined as the second moment of the distribution that represents the beam in each of the two transverse, two-dimensional, subspaces of the four-dimensional phase space. Consider a normalized stationary or non-stationary distribution (x, x') in two-dimensional transverse phase space. The second order moment in the particle coordinate x is defined by:

$$\overline{x^2} = \iint x^2 \rho(x, x') dx dx' \tag{15}$$

The *rms* beam width is then given by:

$$x_{rms} = \tilde{x} = \left(\overline{x^2}\right)^{1/2} \tag{16}$$

In a similar fashion the other second moments is given by:

$$\overline{x'^2} = \iint x'^2 \rho(x,x')dxdx' \tag{17}$$

$$\overline{xx'} = \iint xx' \rho(x,x')dxdx' \tag{18}$$

For normalisation:

$$\iint \rho(x,x')dxdx' = 1 \tag{19}$$

The term $\overline{xx'}^2$ reflects a correlation between x and x′, which occurs when the beam is either converging or diverging (e.g. after passing through a waist). This term is zero at a waist. Two definitions for the rms emittance are commonly used, and they differ by a factor of four for the same phase space distribution:

$$\varepsilon_{rms} = \left(\overline{x^2}\,\overline{x'^2} - \overline{(xx')}^2 \right)^{1/2} \tag{20}$$

and

$$\varepsilon_{4rms} = 4\left(\overline{x^2}\,\overline{x'^2} - \overline{(xx')}^2 \right)^{1/2} \tag{21}$$

For a beam with uniform particle density for which both space charge and external forces are linear (i.e. proportional to the particle's displacement from the axis), the ratio of the total emittance to the rms emittance, $\varepsilon_t / \varepsilon_{rms} = 4$. This ratio is a measure of the tails in the distributions, i.e., how far the particles are spread out in the phase space compared to the rms area. For non-uniform particle distributions the total phase-space area, comprising all particles is generally larger than $\varepsilon_x = 4\varepsilon_{rms}$. However, in most cases of practical interest the fraction of the beam outside this area is relatively small. It is therefore meaningful to use ε_x, which is four times the rms-value of the emittance as a measure of the overall beam quality, following a proposal by Lapostolle [**LAP71**]. For a gaussian distribution, 86% of the beam is contained within the rms-ellipse described by $\varepsilon_{4\,rms}$.

The concept of emittance offers yet another source of confusion. The emittance of a beam will shrink if the beam is further accelerated, because the longitudinal velocity increases without increasing the transverse velocity. To take this into account the normalised emittance ε_n, is used and defined as:

$$\varepsilon_N = \beta\gamma\varepsilon \tag{22}$$

where ε is the emittance of the beam, $\beta = v/c$ the ratio of the particle velocity to the velocity of light in vacuum, and $\gamma = (1-\beta^2)^{-1/2}$.

For an axially symmetric beam it is sufficient to specify the beam properties in one phase-space, for instance x-x'. However, in many cases, e.g. in a beamline with quadrupole magnets, two planes of symmetry have to be used. The emittance ε_y specifies the projection of the four-dimensional transverse phase space distribution on the y-y' plane

In the case of bunched beams, the longitudinal phase space properties have to be included to obtain a complete description of the overall beam quality in the six-dimensional phase space.

The emittance as defined here, is an incomplete description of the beam due to the fact that the particle density in the phase space is not uniform and decreases at the beam edges. It should therefore be specified which fraction of the beam particles lies within a given area in phase space. Presenting the data in a contour map, in which different curves correspond to different fractions of the beam, does this.

7.3 MEASUREMENT OF BEAM EMITTANCE

The method used to measure the emittance of the beam from the duoplasmatron ion source is schematically illustrated in **figure 7.1**. As shown in the figure, the first slit intercepts a large part of the beam and allows a narrowly defined beam with a small

angular divergence to proceed a distance l downstream to the second slit. The current density profile of this narrow beam is determined by scanning the second slit across the beam while the current transmitted by the second slit is measured as a function of the slit position with a Faraday cup. This procedure is repeated for different positions of the first slit. Each position of the first slit defines an x-coordinate within the primary beam as shown in **figure 7.1**.

The angular divergence of the beam passing through the first slit is obtained from the width of the associated current density distribution at the second slit, measured as explained above at a distance l from the first slit. For any given current density level, at the second slit, for example 10% of the highest value, two points at a distance d_1 and d_2 from the axis are defined. The corresponding angle θ, or slope x', is given by the geometric relation $\tan \theta_1 \approx \theta_1 = (d_1 - x_1)/l = x_1'$, and similarly for θ_2.

Plotting the two angles for each position of the first slit in an (x, x')-phase space, yields the closed curve shown in **figure 7.1** (b). The area enclosed by this curve is the emittance for the fraction of the beam defined by the given intensity level. Such emittance contours can be obtained for any fraction of the beam current density distribution. Specifically, the contour corresponding to the zero current density points at the bottoms of each curve, for the beam passing through the first slit, define the total, or 100%, phase space area of the beam. Similarly one can construct phase space contours for 90% and 80% of the beam current. This contour map then provides a good indication of the particle distribution in the (x, x') phase space.

The emittance of the ion source was measured with two slits and a Faraday cup, as described above. The energy of the beam from the source was 12 keV and the beam intensity after the analysing magnet was 60 μA. The position of the emittance-measuring device is after the analysing magnet. The beam intensity distribution for the all the

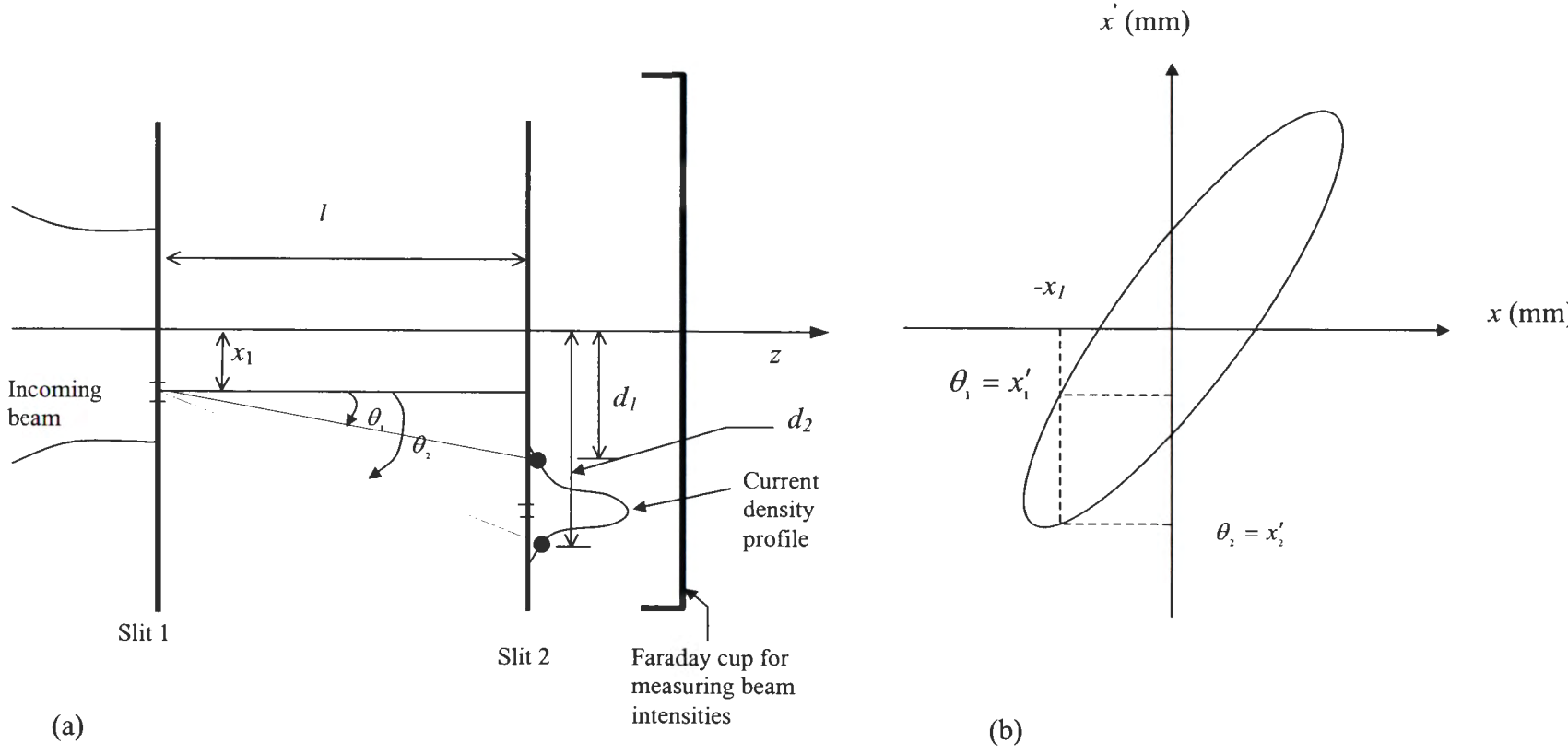

Figure 7.1: (a)-Schematic diagram of the emittance measuring system used to measure the emittance of the source (b)- The phase ellipse for the beam.

different positions of the two slits is shown in **figure 7.2**. The intensity profile of the beam at the second slit is also shown in **figure 7.3**.

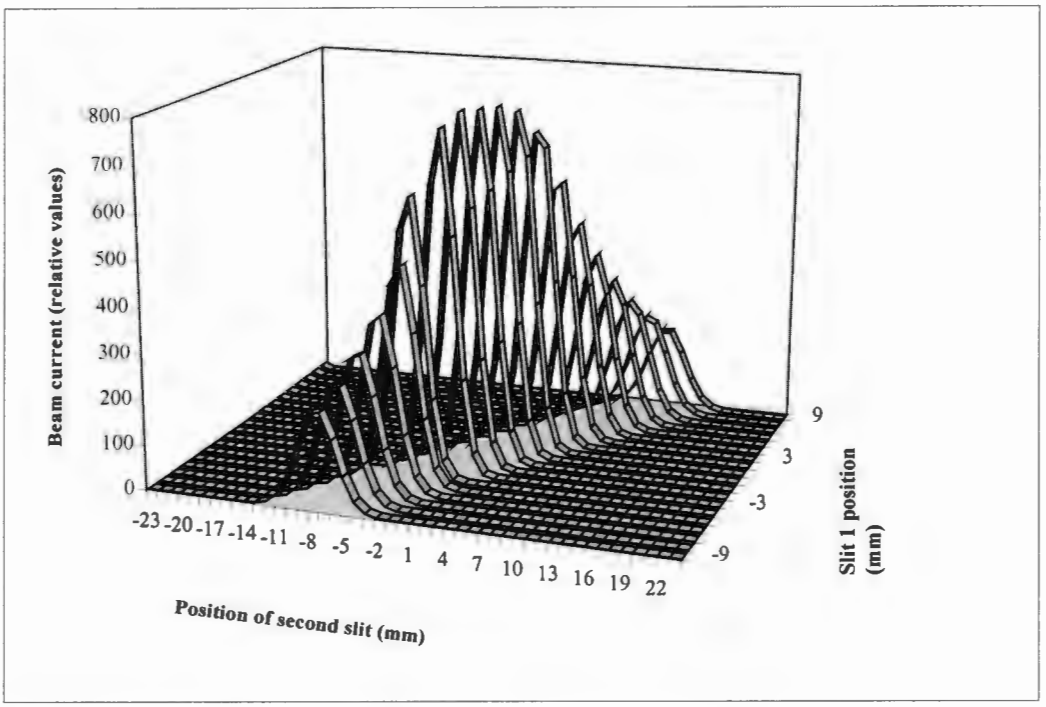

Figure 7.2: The beam intensity distribution for the different positions of the two slits.

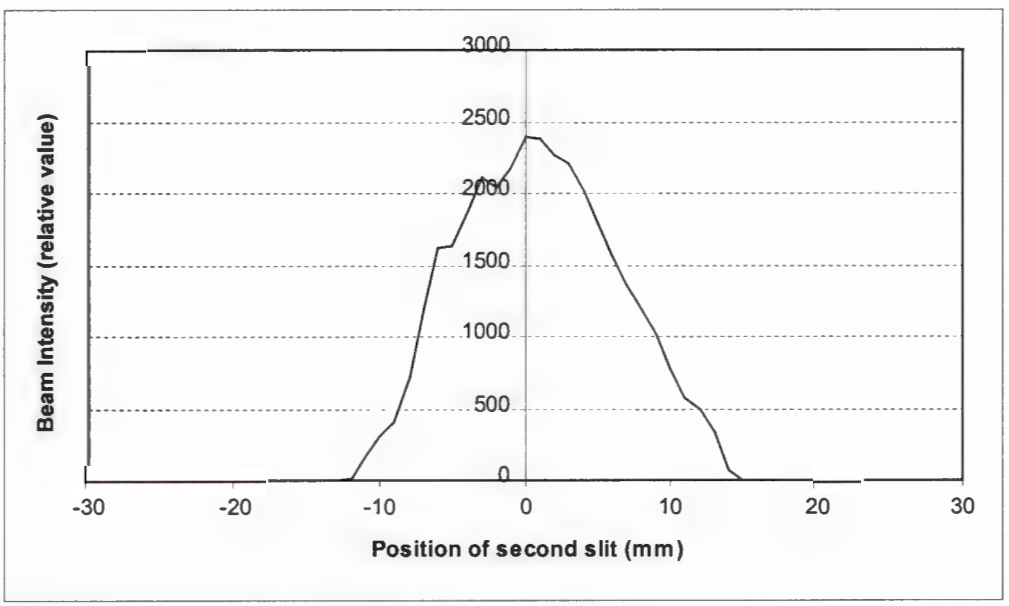

Figure 7.3: The intensity profile of the beam at the second slit.

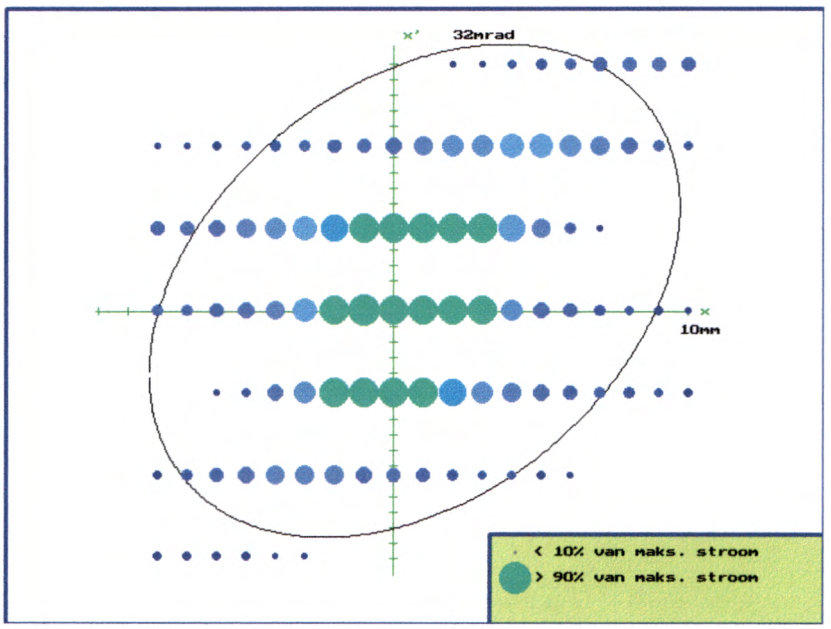

Figure 7.4: The phase ellipse of the beam with 86% of the beam included the ellipse with x-center = 0.697 mm, x' -center = 2.517 mrad, x_{max} = 9.025 mm and x'_{max} = 31.902 mrad.

The phase ellipse of the beam is shown in **figure 7.4**. The measured emittance for 86% of the beam intensity is 270 π mm mrad. By scaling the emittance to a beam energy of 16 keV, the energy for injection into SPC2 for neutrontherapy and isotope production, a value of 234 π mm mrad is obtained and the normalized emittance, ε_N, value is 1.367π mm mrad.

The emittance from the source depends to a large extent on the geometry of the extraction system, which has to be modified for further optimisation of the source.

CHAPTER 8

8.1 CONCLUSIONS

A cold, hollow cathode duoplasmatron ion source has been designed, built, optimized and evaluated for use as an external stand-by ion source for the second injector cyclotron, SPC2, during those times that the light-ion injector cyclotron, SPC1, is out of operation and not available for neutrontherapy and the production of radioisotopes. It could also be used for the Van de Graaff accelerator.

After construction, and commissioning of the peripheral equipment such as the vacuum system, diagnostic equipment, power supplies and other services, the source could, without a major effort, be brought successfully into steady and reliable operation. Minor adjustments to the gas flow and cathode voltage are necessary to ignite the arc in the source. The discharge forms consistently on a day-to-day basis and over a period of months it was found easy to operate the source. The source was operated continuously for up to a week without requiring any maintenance.

The recommended main operating parameters of the duoplasmatron source are summarized as follows:

Gas flow	=	$2.2cm^3/min$
Arc current	=	70mA
Arc voltage	=	70-100V
IE-anode gap	=	5.5mm
IE aperture	=	3.5mm
Anode aperture	=	1mm

These conditions were obtained after extensive optimization of the operating parameters and the most critical source dimensions. The main influences of the parameters and variations in the dimensions are summarized below.

The influence of the operating parameters and critical source dimensions on the source behaviour:

- The beam current increases with increasing anode aperture diameter.
- There exists an optimum IE-anode distance at which the beam current is maximum, beyond that distance the current drops drastically.
- The beam current increases with increasing arc current.
- The beam current increases with increasing extraction voltage.
- There exist an IE opening diameter at which the current peaks and starts dropping beyond that optimum position.
- As the pressure increases, the beam current drops.

It was evident that small changes in operating parameters could result in a significant change in the extracted beam current. In order to understand and explain this behaviour a theoretical study of the factors that influence the performance of the ion source was done. The magnetic field distributions in the source and electron orbit trajectories in the source have been calculated, using the computer program OPERA-3d with the TOSCA module. As can be expected from the complexity of the magnetic field and physical phenomena that takes place in the source, the behaviour of the source could only be explained to some extend. Valuable insight was nevertheless obtained.

An improvement on the extracted beam current was registered after a thin copper layer was fixed on the anode.

A beam current of 80 μA for protons could consistently be obtained for protons, but due to cooling limitations, it is not suitable for periods of more than an hour. A 12 keV proton beam current of between 40-60μA, with a beam emittance of 270 π mm mrad can be continuously extracted from the source, without any heating complications. The proton beam intensity is insufficient for neutrontherapy and production of radioisotopes but suitable for use with the Van de Graaff accelerator and more than what is required for protontherapy and nuclear physics research.

The small physical dimensions of the source were a limiting factor during the optimization process. Probes could not be inserted in the source and voltages and currents had to be limited to prevent sparks and overheating. A source with larger dimensions may be easier to optimize and may give higher currents.

Finally, it has to be concluded that a hollow cold cathode duoplasmatron source, of simple construction and without forced cooling, does not satisfy the beam intensity requirements of neutron-therapy and production of radioisotopes at *i*Themba LABS. This definite result now warrants further consideration for more complex and elaborate ion sources with the certainty that simpler and cheaper solution has been eliminated. However, the study improved the understanding of plasma ion sources at *i*Themba LABS significantly. The skills and knowledge derived from this study can be further applied in future projects of this kind.

REFERENCES

[ABD90] Abdelaziz E. M. The ion sources research and development at the Egyptian Atomic Energy Authority, *Rev. Sci. Instr.* Vol. 61, No. (1) p. 457-459 (1990).

[ABR71] Abroyan M.A. et.al. Duoplasmatron parameters for optimum positive or negative ion yield, *Particle accelerators*, Vol. 2, p. 133-139 (1971).

[ANG83] Angert N. Keller R. and Muller M. Duoplasmatron and PIG ion sources for heavy ions, *Proc. of Intern. Ion Eng. Congress,* p. 225 (1983).

[ANT86] Antaya T.A. The development of a discharge heated Penning Ion source for the multiply charged ions in a K=500 super conducting cyclotron, Ph. D-Thesis, Michigan State University, (1986)

[ARD56] Ardenne M. Atomkernenergie, Vol. 1, 121 (1956).

[BAT74] Batalin V. A. et.al. Duoplasmatron type source with cold cathode, *IEEE Trans. Nucl. Sci.*, Vol. NS 23, No. (2), p. 1097 (1974).

[BEN72] Bennet J. R. J. A review of PIG sources for multiply charged heavy ions, Int. conf. On Ion Sources, *IEEE Trans. Nucl. Sci.*, Vol. NS-19 No. (2), p. 48 (1972).

[BRO89] Brown I.G. The physics and technology of ion sources, *A Wiley-Interscience Publication*, John Wiley and Sons, New York, p. 158 (1989).

[CHE74] Chen F.F. Introduction to Plasma Physics, Plenum Press, New York (1974).

[CON92] Conradie J.L. Improved Proton beam quality and intensity from a 200MeV Cyclotron system, Ph. D-Thesis, University of Stellenbosch, (1992).

[GEL76] Geller R. Electron Cyclotron Resonance multiply charged ion sources, Int. conf. On Ion Sources, *IEEE Trans. Nucl. Sci.*, Vol. NS-23 No. (2), p. 907 (1976).

[GEL96] Geller R. Electron Cyclotron Resonance Ion sources and ECR plasmas. Institute of Physics Publishing Ltd, London (1996).

[GUT49] Guthrie A. and Wakerling R. K. The characteristics of electrical discharges in magnetic fields. McGraw-Hill, USA (1949).

[HIL] Hill C. E. Ion and electron sources, Unpublished.

[KER92] Kerkow H., et.al. A cold cathode ion source with a magnetic hollow cathode, *Nucl. Instr. And Methods*, Vol. B68, p.41 (1992).

[KIS65] Kistemaker J., et.al. Some plasma physical aspects of mono- and duoplasmatron ion sources, *Nucl. Instr. and Methods,* Vol. 38 p. 1-11 (1965).

[KOL98] Kolomities A. Test of duoplasmatron with cold cathode for CW operation, *IEEE Trans. Nucl. Sci.*, p. 2735-2736 (1998).

[KOV71] Kovarik V. and Sluyters Th. An analytical approach to the design of a plasma expansion cup, *IEEE Trans. Nucl. Sci.,* p. 21(1971).

[LAP71] Lapostolle P. M. Possible increase through filamentation due to space charge in continuous beams, *IEEE Trans. Nucl. Sci.*, Vol. NS-18, p. 1101 (1971).

[LEJ71] Lejeune C. Theoretical and experimental study of the gas efficiency in a duoplasmatron ion source, *IEEE Trans. Nucl. Sci.,* p. 27 (1971).

[LEJ74I] Lejeune C. Theoretical and experimental study of the duoplasmatron ion source, Part 1: Model of a duoplasmatron discharge, *Nucl. Inst. And Methods*, Vol. 116, p. 417-428 (1974).

[LEJ74II] Lejeune C. Theoretical and experimental study of the duoplasmatron ion source, Part 2: Emissive properties of the source, *Nucl. Inst. And Methods*, Vol. 116, p. 429-443 (1974).

[MAI02] Maine P. Design and optimization of the beamline between an external duoplasmatron ion source and the second solid-pole injector cyclotron (SPC2) at *i*Themba LABS, M Sc (ARST)-Dissertation, University of North West, (2002).

[MAH58] Mahaffey D.W, et.al. Beam-plasma interactions, *Phys. Rev.*, Vol. 112, p.1052 (1958).

[MIN87] Ma Mingxiu, et.al. Hollow cathode multipurpose ion source, *Nucl. Instr. and Methods*, Vol. B21, p. 182 (1987).

[QAY94] Qayyum A. and Ahmad S. A magnetically confined hollow cathode duoplasmatron for the PINSTECH ion implanter, *Nucl Instr. And Meth. In Phys. Res.*, Vol. B94 p. 597-600 (1994).

[RAU75] Rautenbach W. L, and Botha A. H. Proposal for a South African National Accelerator Facility for physics and medicine, *7th Intern. Conf. On Cyclotrons and their Applications*, Birkhäuser, Basel, p. 117-120 (1975).

[REP75] Report on the requirements for and the choice of a National Accelerator Facility for the Republic of South Africa and the Placing thereof, unpublished (1975).

[SCH97] Schmidt C. W. Duoplasmatron source modification for $^{3}He^{+}$ operation, *Rev. Sci. Instr.*, Vol. 69, No. (2) p. 1020-1023 (1998).

[TON85] Tonegawa A. et.al. Simple hollow cathode ion source, *Nucl. Instr. and Methods*, Vol. B6, p. 129 (1985).

[TON87] Tonegawa A. et.al. Plasma compression type hollow cathode ion source, *Nucl. Instr. and Methods*, Vol. B21, p. 212 (1987).

[ZHO81] Zhon B. and Yan H. A duoplasmatron ion source for solid materials such as As and P, *Nucl. Instr and Methods*, Vol. 189 p. 335-339 (1981).